



Early Paleozoic magmatism and metallogeny related to Proto-Tethys subduction: Insights from volcanic rocks in the northeastern Altyn Mountains, NW China



Cheng-Ming Wang ^{a, b, *}, Hao-Shu Tang ^{c, **}, Yi Zheng ^{a, b}, Lian-Hui Dong ^d, Ji-Hong Li ^d, Xun Qu ^d

^a School of Earth Sciences and Engineering, Sun Yat-sen University, Guangzhou 510275, China

^b Guangdong Provincial Key Lab of Geodynamics and Geohazards, Sun Yat-sen University, Guangzhou 510275, China

^c State Key Laboratory of Ore Deposit Geochemistry, Institute of Geochemistry, Chinese Academy of Sciences, Guiyang 550081, China

^d Bureau of Xinjiang Geology and Mineral Resources Development, Urumqi 830000, China

ARTICLE INFO

Article history:

Received 2 September 2018

Received in revised form

11 April 2019

Accepted 18 April 2019

Available online 7 June 2019

Keywords:

Proto-Tethys

Altyn Mountains

Volcanic rocks

Tectonic setting

Metallogeny

ABSTRACT

Remnants of the Proto-Tethys are mainly preserved in the region between south of the North China-Tarim Block and north of Qiangtang-Sibumasu/Baoshan Blocks. Magmatic-metallogenetic events related to the Proto-Tethyan subductions were rarely reported, and the subduction history and polarity of the Proto-Tethyan are still under debate. Here, we presented new data of zircon U–Pb ages, whole-rock Sr–Nd–Pb isotopes, major and trace elements and zircon Hf isotopes for the volcanic rocks in the northeastern Altyn Mountains. Information of over 14 volcanic-hosted deposits/prospects in the region has been compiled. These volcanic ore hosts consist mainly of basaltic andesite, andesite, dacite and rhyolite rocks. The andesite and rhyolite rocks are newly zircon U–Pb dated to be Late Cambrian-Early Ordovician (andesite: 490.5 ± 5.2 Ma; rhyolite: 492.6 ± 2.9 Ma and 491.6 ± 5.6 Ma), representing the timing of volcanism and VMS (Volcanogenic Massive Sulfide) mineralization. All the volcanic rocks belong to the high-K calc-alkaline and shoshonite series: the andesite rocks from the Kaladawan area in north of the region display arc geochemical affinities and contain $(^{87}\text{Sr}/^{86}\text{Sr})_i$ (0.7082 – 0.7083) and $\epsilon_{\text{Nd}}(t)$ (-9.7 to -7.6), indicating that they were likely formed by partial melting of the mantle wedge with subducted sediment inputs. The rhyolite rocks from the Kaladaban area in south of the region are characterized by high SiO_2 (64.46 – 78.55 wt%), low alkali ($\text{Na}_2\text{O} + \text{K}_2\text{O}$, 3.46 – 7.17 wt%), and contain $(^{87}\text{Sr}/^{86}\text{Sr})_i$ (0.7063 – 0.7095), $\epsilon_{\text{Nd}}(t)$ (-6.6 to -1.5), and zircon $\epsilon_{\text{Hf}}(t)$ (-5.5 to 5.4), indicating that they were likely derived from partial melting of the lower crust with depleted mantle inputs. Rock assemblage and geochemistry suggest that volcanic rocks in the northeastern Altyn Mountains may have formed in a continental arc setting. Their spatial distributions with respect to the ophiolites in the region suggest that the subduction was likely south-dipping. This subduction-related arc magmatism may have formed the many important VMS and porphyry-skarn deposits in the region.

© 2019 International Association for Gondwana Research. Published by Elsevier B.V. All rights reserved.

1. Introduction

The Proto-Tethys Ocean, whose geological records mainly distributed in East Asia (Zhong, 1998), has been defined as “an ancient ocean extending from the Tarim-North China Block to the north, to the South Qiangtang-Sibumasu/Baoshan Blocks to the south (Fig. 1a, b). It opened due to the breakup of the Rodinia Supercontinent since the Neoproterozoic and closed due to the

assembly of the Gondwana Supercontinent at the end of the Early Paleozoic” (Chen, 1994; Guo, 2001; Li et al., 1990, 1991, 2010a, 2010b, 2017b; Li and Yin, 2002; Lu, 2001; von Raumer and Stampfli, 2008; Xiao et al., 2003, 2009; Zhang et al., 2012; Zhao et al., 2015). The Proto-Tethyan subductions and the subsequent (micro)-continental accretions are recorded by a series of early Paleozoic ophiolites and HP-UHP (High Pressure-Ultra High Pressure) metamorphic rocks in several Early Paleozoic orogenic belts of China, e.g., the North Qinling Orogen (Cao et al., 2016; Dong et al., 2011a, 2011b), the North Qilian Orogen (Feng et al., 1994; Ge and Liu, 1999; Liu et al., 2016; Song et al., 2013; Xia et al., 1996, 2003; Xiang, 1982; Z.C. Zhang et al., 2001; Zuza et al., 2017), and the Altyn Orogen herein (Xu et al., 2006; Yin et al., 2002; J. Zhang et al., 2015b). Understanding the Proto-Tethyan evolution is important for the

* Correspondence to: C.M. Wang, School of Earth Sciences and Engineering, Sun Yat-sen University, Guangzhou 510275, China.

** Corresponding author.

E-mail addresses: wangchengming0216@163.com (C.-M. Wang), tanghaoshu@vip.gyig.ac.cn (H.-S. Tang).

Pangaea supercontinent reconstruction (W. C. Li et al., 2010b), however, the Proto-Tethyan subduction history and polarity are still controversial, partly due to the subsequent multi-phase tectonic overprinting the original structures. Besides, these orogenic belts contain a number of important volcanic-hosted precious/base metal deposits, yet rare previous researches had been investigated the possible metallogenic linking with the Proto-Tethyan tectonics.

The Altyn Mountains are situated between the Tarim and Qaidam Basins (Fig. 1b, Sobel and Arnaud, 1999). It were likely formed by multiple phases of subductions and collisions, which are now preserved as fragments of island arcs, accretionary prisms, ophiolites, seamounts, and HP/UHP metamorphic rocks (Che et al., 1995; Chen et al., 2011, 2016; Sobel and Arnaud, 1999; Sun et al., 1997; Yang et al., 2002a, 2002b; Yang and Xu, 2002; J. Zhang et al., 2001; Zhang et al., 2007). The Altyn Mountains comprises four tectonic units (from north to south) (Fig. 1b), including: the Northern Altyn Block (NAB), Northern Altyn Subduction Complex (NASC), Central Altyn Block (CAB) and the Southern Altyn Subduction–Collision

Complex (SASCC) (Liu et al., 1999; Xu et al., 1999). Among them, the NASC (about 200 km long and 5–15 km wide) contains the deformed vestiges of arcs and ophiolite complexes preserved in the northern part of the Proto-Tethys Ocean, which were accreted onto either the NAB or CAB (depending on different theories of subduction polarity) during the ocean closure in the Ordovician (Che et al., 1995; BChen et al., 2009b; Chen et al., 2015; Gehrels et al., 2003; Liu et al., 1999; Yang et al., 2008; Zhang et al., 2005).

The NASC hosts the majority of mineral occurrences in the Altyn Mountains, notably famous the Kaladawan district in the eastern NASC (Fig. 1c). In the Kaladawan district, deposits discovered during recent decade including the Kaladawan Fe–Mo and Baijianshan Fe ore fields, the Kaladaban Zn–Pb and Kaladawan Cu–Pb–Zn deposits (Wang et al., 2017, 2018a,b). These deposits contain total metal reserves of 200 Mt Fe, 1 Mt Zn and 0.5 Mt Pb. Most of these Cu–Zn–Pb deposits are volcanic-hosted, therefore, the NASC volcanic rocks can shed light on the tectonic evolution and metallogeny of the NASC, as well as the Altyn Mountains as a whole.

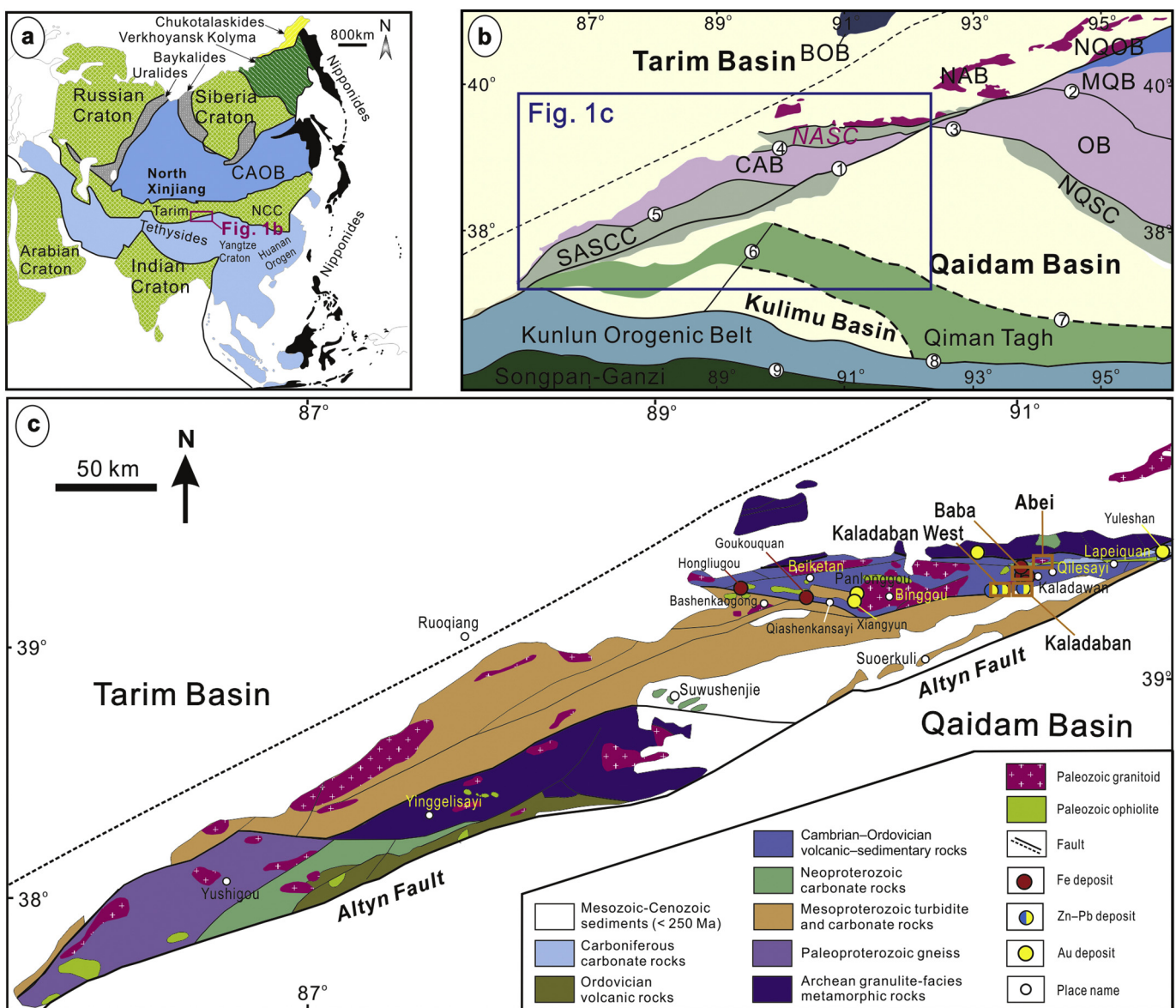


Fig. 1. (a) Tectonic framework of the Eurasian continent, showing the location of the Altyn Mountains (modified after [Şengör and Natal'in, 1996](#)). (b) Tectonic map of the Altyn Mountains ([He et al., 2004](#)). (c) Simplified geologic map of the Altyn Mountains, showing the location of the Kaladawan district ([He et al., 2004](#)). Abbreviation: BOB: Beishan Orogenic Belt; NQOB: Northern Qilian Orogenic Belt; MQB: Middle Qilian Block; OB: Oulongbuluke Block; NQSC: Northern Qilian Subduction Complex. Faults: 1 Altyn Fault, AF; 2 Northern Altyn Marginal Fault, NAMF; 3 Northern Qaidam Fault, NQF; 4 Jinyanshan thrust Fault, JTF; 5 Aihemaiti-Kaoshi Kantugai Fault, AKKF; 6 Baiganhu Fault, BF; 7 Northern Kunlun Fault, NKF; 8 Central Kunlun Fault, CKF; 9 Southern Kunlun Fault, SKE.

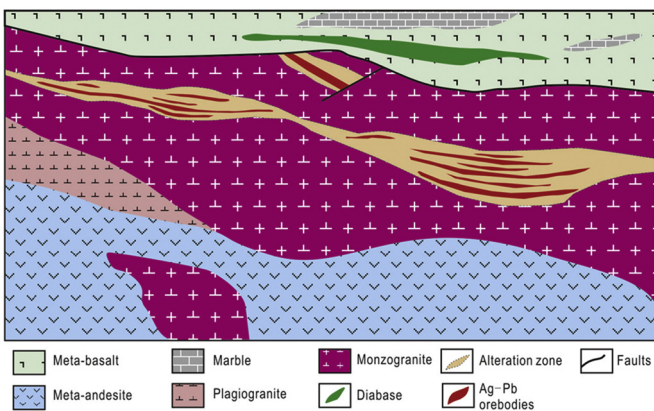


Fig. 2. Geological map of the Abei Ag–Pb deposit.
(Modified after Chen et al., 2012.)

However, the ages of those volcanic rocks and the volcanic-hosted mineralization have not been well constrained (Cui, 2010; Li et al., 2013). The tectonic setting has been variably attributed to be island arc or continental arc (Cui, 2010; Li et al., 2013), or collisional-related (Hao et al., 2013). These geotectonic controversies are partly caused by the lack of detailed geochemical (including Sr–Nd–Hf isotopes) data.

In this paper, we reported new data on zircon U–Pb ages, whole-rock geochemistry and Sr–Nd–Pb isotopes, and zircon Hf isotope data for the volcanic rocks in the Kaladawan district. Consequently, we will discuss: (i) the petrogenesis of these volcanic rocks; and especially, (ii) the possible tectonic setting and its polarity concerns with the Proto-Tethyan subduction; as well as (iii) any metallogenic links with the volcanic-hosted precious/base-metal deposits.

2. Geological setting

2.1. Regional geology

The Altyn Mountains are suggested to have been influenced by at least six major tectonic episodes (X. Chen et al., 2009b; Liu et al., 2009): 1) Development of the Archean–Paleoproterozoic continental basement; 2) Deposition of the Mesoproterozoic platform sedimentary rocks; 3) Neoproterozoic continental rifting and formation of the Proto-Tethys; 4) Paleozoic subduction and closure of

the Proto-Tethys; 5) Mesozoic N–S-trending extension (Chen et al., 2003a, b); 6) Cenozoic strike-slip shearing of the Altyn Fault.

The NASC is sandwiched between the NAB and CAB Precambrian continental blocks (Fig. 1c). The NAB is considered to be the Archean–Paleoproterozoic basement of the Tarim Craton, and composed mainly of Archean high-grade metamorphic rocks (e.g., granitic gneiss, granulite and migmatite) with minor Neoproterozoic sedimentary rocks (Xin et al., 2013). The CAB comprises Neoarchean–Paleoproterozoic basement rocks (e.g., biotite–plagioclase–amphibole schist, biotite–plagioclase gneiss, garnet–amphibolite and biotite granulite, and metamorphosed tonalite and granodiorite) and weakly metamorphosed Mesoproterozoic–Neoproterozoic clastic and carbonate rocks (Wang et al., 2002). The NASC consists of variably deformed and metamorphosed Neoproterozoic–Paleozoic sedimentary, volcanic and plutonic rocks, ophiolites and high pressure metamorphic rocks (Che et al., 1995; Chen et al., 2001; Yang et al., 2008).

In the Kaladawan district, exposed strata of the NASC include: i) the Neoproterozoic Suolake Formation (ca. 0.80–0.68 Ga; Xinjiang BGMR, 2009a) low-grade metamorphosed volcanic–siliciclastic–carbonate rocks; ii) the Cambrian Tashibulake Formation low-grade metamorphosed volcanic-sedimentary rocks; iii) the Ordovician Kaladawan Formation low-grade metamorphosed marine volcanic rocks (with minor sedimentary rocks); and iv) the Carboniferous Yingebulake Formation carbonate and clastic rocks (B. Chen et al., 2009). The Tashibulake and Kaladawan Formations are intruded by many Paleozoic rocks, including mainly diorite, granodiorite, monzogranite and granite, and minor dolerite and gabbro. Han et al. (2012) divided the Paleozoic magmatism in the Kaladawan district into the pre-collision (ca. 520–500 Ma), syn-collision (ca. 490–470 Ma) and post-collision (ca. 440–410 Ma) phases. Furthermore, some ophiolitic fragments are distributed to the east of the Kaladawan district and exhibit faulted contacts with the Paleozoic sequences. These ophiolitic fragments are mainly consisted of mantle peridotite, mafic–ultramafic rocks, sheeted dikes and basaltic lavas (Yang et al., 2008). Gabbro from the ophiolite yielded a zircon SHRIMP U–Pb age of 479.4 ± 8.5 Ma (Yang et al., 2008).

Most of the outcropping volcanic rocks in the Kaladawan district of the NASC were named the Kaladawan Formation according to the 1:250 k geologic map (Xinjiang BGMR, 2008), with the lithologies including mainly meta-basalt, meta-basaltic andesite, meta-dacite, meta-rhyolite, volcanic breccia, agglomerate and tuff. This paper focused on the volcanic rocks in the southern part of the Kaladawan district, which host most of the Zn–Pb–Cu deposits/occurrences, e.g., the Kaladaban and Cuiling Zn–Pb deposits, and Kaladaban West Cu–Zn–Pb deposit (Fig. 1c).

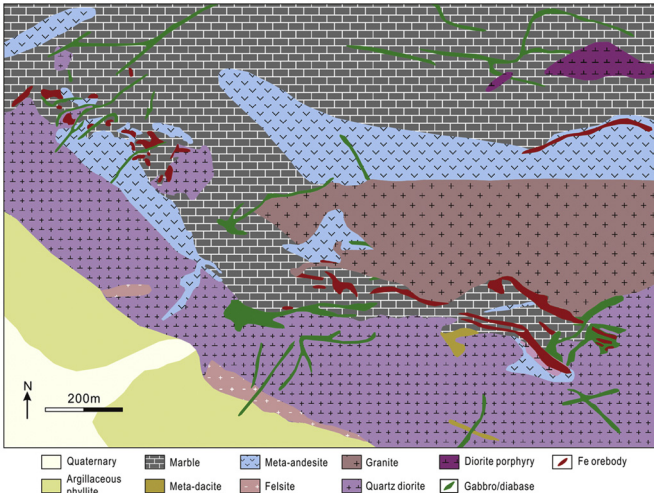


Fig. 3. Geological map of the Baba Fe deposit (Xinjiang BGMR, 2012a).

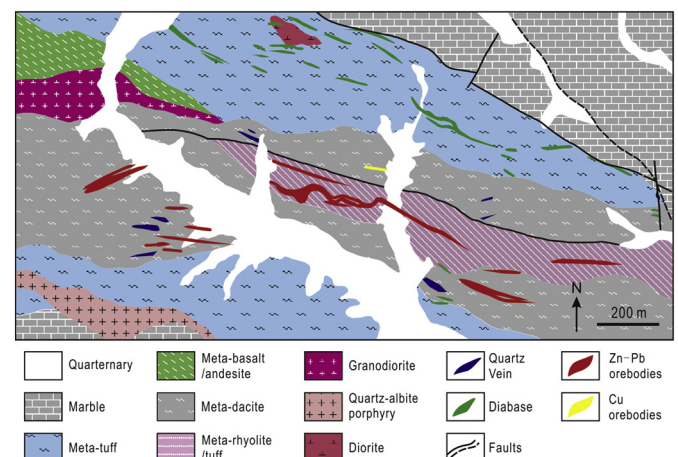


Fig. 4. Geological map of the Kaladaban Zn–Pb deposit (Xinjiang BGMR, 2012b).

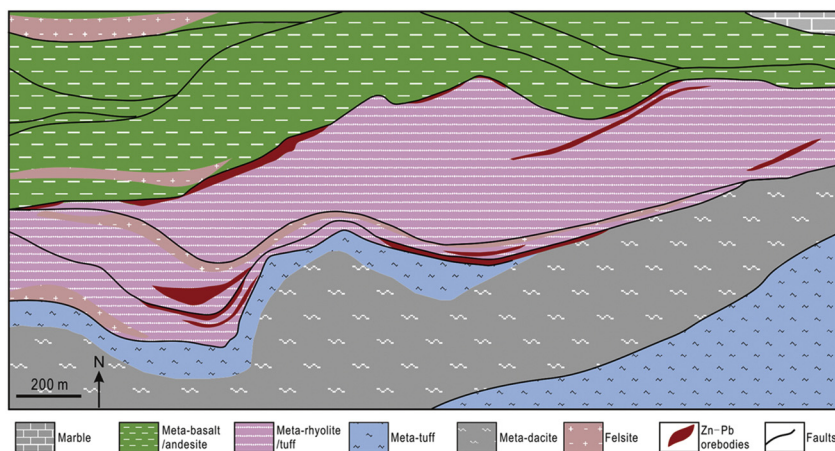


Fig. 5. Geological map of the Kaladaban West Cu–Zn–Pb deposit (Xinjiang BGMR, 2013).

2.2. Characteristics of typical mineral deposits

2.2.1. Abei Ag–Pb deposit

The Abei Ag–Pb deposit is spatially associated with monzogranites intruding into Early Paleozoic meta-basalt, andesite and marble (Fig. 2). Orebodies are veined and lenticular, and controlled by NWW/EW-trending brittle fault zones. Ores are massive, disseminated and veined. Ore minerals include argentite, galena, pyrargyrite, sphalerite, chalcopyrite and pyrite. Gangue minerals are quartz, calcite, sericite and chlorite. Mineralization-related alterations include silicic, sericite, chlorite alterations. Although sulfur isotopes ($\delta^{34}\text{S} = 11.9\text{--}16.3\text{\textperthousand}$) suggested mixed marine sedimentary and magmatic sulfur sources, Chen et al. (2012) insisted that the Abei deposit was magmatic hydrothermal mineralization related to the intrusion of the monzogranites.

2.2.2. Baba Fe deposit

The Baba Fe deposit is a medium-size deposit in the east of the Kaladawan Fe–Mo orefield. Exposed strata in the deposit include the Early Paleozoic marble, carbonaceous slate, sericite phyllite, meta-andesite and meta-dacite (Fig. 3). These rocks were first intruded by gabbro and dolerite dike swarms, folded and then intruded by the Kaladawan diorite porphyry, granodiorite and granite. The granite intrusion is E-trending, parallel to the major structural line of the district. It is U–Pb dated to be the Early Ordovician (476.1 ± 3.3 Ma) and attributed to highly fractionated I-

type granite based on geochemical characters (Wang et al., 2018a). Alterations associated with the granite show a distinct zoning pattern from the granite outward: garnet + pyroxene skarns, to magnetite + molybdenite associated with epidote + actinolite \pm tremolite skarns, to epidote + calcite \pm wollastonite hornfels. Orebodies are mainly hosted in skarns and contain magnetite and molybdenite. The majority of magnetite mineralization occurs along the intrusive contact zones. The high grade iron orebodies are usually hosted in retrograde skarns mainly comprising of epidote, tremolite and actinolite. Quartz/calcite–molybdenite veins cross-cut the skarns. Other metallic minerals present include pyrrhotite, pyrite, chalcopyrite, sphalerite, galena and scheelite. Gangue minerals include mainly garnet, diopside, tremolite, actinolite, epidote, zoisite, chlorite and calcite. Wang et al. (2018a) proposed that the Fe–Mo mineralization at Kaladawan (including Baba) was a typical skarn deposit related to the Kaladawan granite intrusion.

2.2.3. Kaladaban Zn–Pb deposit

The Kaladaban Zn–Pb deposit is situated north of the Jinyanshan Fault. Exposed rocks in the deposit include mainly the Early Paleozoic metamorphosed volcanic rocks, i.e., basalt, andesite, dacite, rhyolite and tuff (Fig. 4). Orebodies are stratiform/lenticular in the metamorphosed volcanic rocks. The economically significant stratiform massive orebodies are mainly distributed in the upper part of the ore-hosting horizons while the less important vein-type orebodies are distributed in the lower part (stockwork zone). The

Table 1

Descriptions of volcanic rock samples in southern Kaladawan district.

Sample number	Rock type	Lat. (E)	Long. (N)	Sample description
Kaladawan area				
KFP-42	Basaltic andesite	91°44'37.10"	39°05'15.22"	Dark-grey, porphyritic texture, consisting of plagioclase (45–65%), hornblende (5%) and some cryptocrystalline-glassy material (30–50%). Major phenocrysts: hornblende and plagioclase.
KFP-56		91°44'40.29"	39°05'21.06"	Groundmass: cryptocrystalline texture, the chief matrix mineral is plagioclase (40%–60%).
KFP-57		91°44'41.16"	39°05'22.56"	Accessory mineral: magnetite and ilmenite.
KFP-34	Andesite	91°44'32.38"	39°05'09.04"	Grey, aphanitic texture (Fig. 6c), consisting of plagioclase (45–65%), hornblende (5%) and volcanic glass (30–50%). Accessory minerals: magnetite and epidote.
KFP-39		91°44'35.58"	39°05'13.01"	
KFP-43		91°44'37.38"	39°05'19.05"	
KFP-35	Dacite	91°44'32.65"	39°05'11.25"	Light-grey, porphyritic texture, rhyolitic structure. Phenocrysts: quartz and feldspar (10%–15%). Groundmass: microgranular and contains microcrystalline–cryptocrystalline felsic minerals (sericite, chlorite and epidote). Accessory minerals: magnetite and zircon.
KFP-36		91°44'33.34"	39°05'12.40"	
KFP-47		91°44'39.22"	39°05'09.05"	
KFP-53		91°44'38.39"	39°05'20.06"	
Kaladaban Zn–Pb deposit				
KLDB-V1	Dacite	91°48'45.05"	39°04'05.13"	Grey, porphyritic texture, rhyolitic structure (Fig. 6i), comprising plagioclase (25–35%), K-feldspar (30–40%), quartz (10–15%) and volcanic glass (15–25%). Phenocrysts: plagioclase, K-feldspar and quartz.
KLDB-V2		91°48'58.24"	39°04'15.65"	
KWP-1	Rhyolite	91°40'21.96"	39°03'45.73"	
KWP-2		91°40'20.33"	39°03'44.12"	
KBY2-21		91°49'02.77"	39°04'18.23"	
KBY2-21		91°49'05.80"	39°04'20.11"	

deposit is locally intruded by dolerite, diorite, granodiorite and quartz–albite porphyry. Ores are massive, semi-massive, banded, densely disseminated, disseminated, veined or brecciated. Sulfides include mainly pyrite, sphalerite, galena and chalcopyrite, with minor tetrahedrite; and gangue minerals include mainly quartz, barite, chlorite, biotite, muscovite, phlogopite and calcite. Mineralization-related alterations include silicic, sericite, chlorite, barite and carbonate and mainly distributed in the lower part of the hosting rocks.

2.2.4. Kaladaban West Cu–Zn–Pb deposit

The deposit is a large-size Cu–Zn–Pb deposit located in the west of the Kaladaban Zn–Pb deposit. Stratiform and lenticular orebodies are hosted by Early Paleozoic metamorphosed volcanic rocks (Fig. 5). The volcanic rocks strike 85–100° and dip 55°–75° to the north, intruding by subvolcanic rocks (felsite) and albite–quartz porphyries. Faults in this deposit are mainly E/NEE-trending. Ores are banded, semi-massive, disseminated or veined. Ore minerals include mainly pyrite, sphalerite, galena, chalcopyrite,

chalcocite and tetrahedrite. Gangue minerals are mainly quartz, barite, chlorite, biotite, muscovite, phlogopite and calcite. Mineralization-related alterations include silicic, sericite, chlorite, barite and carbonate and mainly distributed in the lower part of the hosting rocks.

3. Sampling and petrology

Most of the intermediate–felsic volcanic rocks in the Kaladaban district have undergone varying degree of chlorite, sericite and carbonate alterations. After petrographic observations, sixteen least-altered samples were selected for whole-rock major and trace

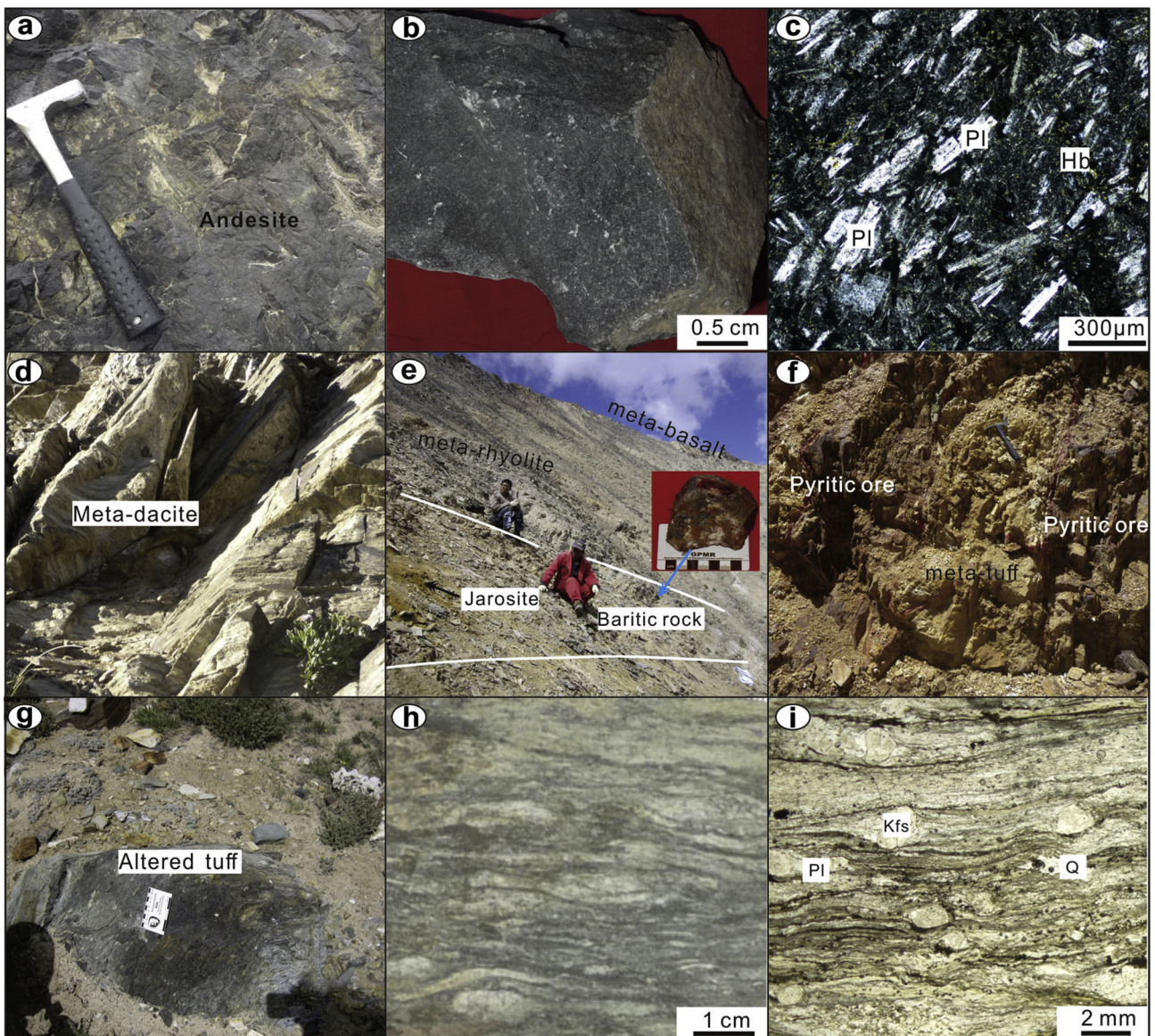


Fig. 6. Representative photos of volcanic rocks in the southern Kaladawan district. Volcanic rocks near the Kaladawan Fe–Mo orefield: (a) Epidote-altered outcrop of andesite; (b) Fresh and massive texture andesite hand specimen; (c) Photomicrographs of andesite. Volcanic rocks in the Kaladawan Zn–Pb deposit, showing the relationship between orebody and volcanic rocks: (d) Meta-dacite in the hanging wall; (e) Layered meta-basalt/rhyolite with baritic rocks; (f) Orebody containing pyritic ores interlayered with meta-tuff; (g) Tuffs with chlorite alteration in the footwall; (h) Hand specimen of fresh rhyolite; (i) Rhyolitic structure. Abbreviations: Kfs—K-feldspar; Qz—Quartz; Pl—Plagioclase; Hb—Hornblende.

element analyses in this study (Table 1). Of these, three samples (KFP-43, KBY2-21 and KBY2-22) were selected for zircon age datings and Hf isotope analyses. Six samples were selected for whole-rock Sr–Nd–Pb isotope analyses. Six intermediate and four felsic volcanic rocks were collected from near the Kaladawan Fe–Mo orefield (north of the Kaladaban district; Fig. 1). Another six felsic volcanic rocks were collected from the Kaladaban Zn–Pb deposit. Detailed descriptions and microscopic photos of collected volcanic rock samples are shown in Table 1 and Fig. 6, respectively.

4. Analytical methods

4.1. Zircon U–Pb dating

The rock samples were crushed into 80–120 mesh, washed and dried. The zircons were separated using conventional heavy liquid and magnetic separation techniques. The zircons with good crystal shape and without cracks were handpicked under a binocular microscope, mounted in epoxy resin and polished to about half their thickness. The zircons were imaged under transmission light and then with cathodoluminescence (CL) to reveal their internal structure and to select the spots for the analyses.

The selected zircons were analyzed by laser ablation inductively coupled plasma mass spectrometry (LA-ICP-MS) at the State Key Laboratory of Continental Dynamics, Northwest University (China). Laser ablation was carried out using a GeoLas 200M system (with 20 μm beam diameter and 10 Hz frequency) coupled with an Agilent 7500a ICP-MS. The Standard SRM610 was used as external standard and ^{29}Si was chosen as internal standard. Zircon 91,500 was used as external standard for U–Pb dating. The analytical uncertainty for the Zircon 91,500 in this study was <2%. Detailed operating conditions for the laser ablation system and the ICP-MS

instrument and data reduction were similar to those of described by Liu et al. (2008). Time-drift correction and quantitative calibration for trace element analyses and U–Pb dating were performed by Glitter (Version 4.0), and the data were reported with a precision better than $\pm 1\sigma$. Concordia diagrams and weighted mean age calculations were made by using Isoplot/Ex_ver3. Weighted mean ages for pooled U–Pb analyses were quoted with 95% confidence interval.

4.2. Whole-rock major and trace elements

Whole-rock major element analyses were performed at the ALS Chemex Laboratory in Guangzhou (China). Major oxides were determined by X-ray fluorescence spectrometry (XRF) on fused glass disks, using the Standard GB/T14506.28-1993 for Na_2O , MgO , Al_2O_3 , SiO_2 , P_2O_5 , K_2O , CaO , TiO_2 , MnO and Fe_2O_3 , the Standard GB/T14506.2-1993 for H_2O^+ , the Standard GB 9835-1988 for CO_2 and the Standard LY/T 1253-1999 for loss-on-ignition (LOI). The precision is estimated to better than 5%.

Rare earth elements (REEs) and trace elements including Cu, Pb, Th, U, Hf, Ta, Sc, Cs, V, Co and Ni were analyzed by using the ELAN6000 ICP-MS at the Analysis Center of Top Resource and Environment (Guangzhou), following the procedures of Qi et al. (2000). The Standard USGS W-2–G-2 and Chinese Standards GSR-1, GSR-2 and GSR-3 were used to calibrate the element contents, with a precision of better than 3%.

4.3. Whole-rock Sr–Nd–Pb isotopes

Whole-rock Sr–Nd isotope analyses were carried out at the State Key Laboratory of Isotope Geochemistry, Guangzhou Institute of Geochemistry (GIG), Chinese Academy of Sciences (CAS). The

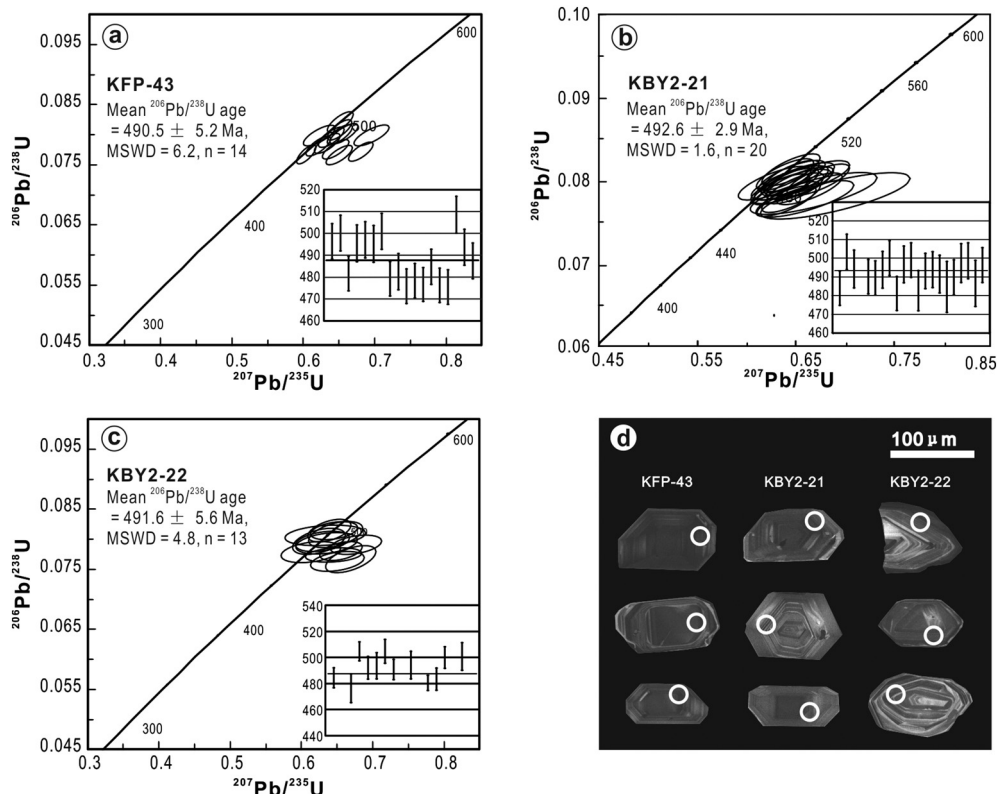


Fig. 7. Zircon U–Pb concordia diagrams (a–c) and representative CL images (d) of the zircons from the volcanic rocks in the southern Kaladawan district. Circles indicate the laser spot locations.

isotopic determination was performed on a Neptune Plus multi-collector (MC)-ICP-MS equipped with nine Faraday cup collectors and eight ion counters. Detailed analytical procedures were similar to Waight et al. (2002) and Yang et al. (2009), respectively. Normalizing factors used to correct the mass fractionation of Sr and Nd during the measurements were $^{86}\text{Sr}/^{88}\text{Sr} = 0.1194$ and $^{146}\text{Nd}/^{144}\text{Nd} = 0.7219$. Analyses of the standards NIST SRM987 and Shin Etsu JNd-1 over the measurement period provided $^{87}\text{Sr}/^{86}\text{Sr} = 0.710288 \pm 0.000005$ (2SD) ($n = 21$) and $^{143}\text{Nd}/^{144}\text{Nd} = 0.512086 \pm 0.000004$ (2SD) ($n = 19$), respectively,

consistent with the values measured by Weis et al. (2006). The background values of Sr and Nd were 2×10^{-10} to 5×10^{-10} and $< 5 \times 10^{-11}$, respectively.

Lead isotopic analysis was also carried out at the State Key Laboratory of Isotope Geochemistry, GIGCAS. The isotope measurements were performed on a Neptune Plus MC-ICP-MS. Samples were doped with Tl and mass discrimination was corrected relative to the certified $^{205}\text{Tl}/^{203}\text{Tl}$ ratio. Detailed analytical procedures were similar to Chernyshev et al. (2007). Analyses of the Standard NIST SRM981 over the measurement period provided $^{206}\text{Pb}/^{204}\text{Pb} = 16.9354 \pm 0.0003$

Table 2

Zircon U–Pb dating results for the volcanic rocks in southern Kaladawan district.

Spots	U (ppm)	Th (ppm)	Th/U (1)	$^{207}\text{Pb}/^{206}\text{Pb}$		$^{207}\text{Pb}/^{235}\text{U}$		$^{206}\text{Pb}/^{238}\text{U}$		$^{207}\text{Pb}/^{206}\text{Pb}$		$^{207}\text{Pb}/^{235}\text{U}$		$^{206}\text{Pb}/^{238}\text{U}$		Concordance (%)
				Ratio (1)	1σ (%)	Ratio (1)	1σ (%)	Ratio (1)	1σ (%)	Age (Ma)	1σ (Ma)	Age (Ma)	1σ (Ma)	Age (Ma)	1σ (Ma)	
KFP-43 (Andesite)																
1	406	267	0.66	0.05899	1.25	0.65113	1.11	0.08004	0.85	566.8	27.1	509.2	4.4	496.4	4.1	97
2	493	281	0.57	0.06342	1.23	0.7056	1.08	0.08068	0.84	722.3	26	542.1	4.6	500.2	4.1	92
3	305	186	0.61	0.06032	1.33	0.64534	1.18	0.07758	0.85	615.1	28.4	505.6	4.7	481.7	4	95
4	529	500	0.95	0.17446	1.36	1.89398	1.2	0.07872	0.91	2600.9	22.6	1079	8	488.5	4.3	45
5	161	68	0.42	0.06314	1.57	0.69557	1.44	0.07989	0.89	712.8	33.1	536.1	6	495.5	4.2	92
6	546	435	0.8	0.05943	1.36	0.65696	1.22	0.08016	0.86	582.9	29.3	512.8	4.9	497.1	4.1	97
7	133	51	0.38	0.05651	1.59	0.62237	1.46	0.07987	0.88	471.5	35.1	491.3	5.7	495.3	4.2	99
8	531	374	0.71	0.05839	1.23	0.65068	1.08	0.08081	0.85	544.3	26.6	508.9	4.3	501	4.1	98
9	499	375	0.75	0.06393	1.19	0.68058	1.03	0.07719	0.84	739.5	24.9	527.1	4.3	479.3	3.9	91
10	518	389	0.75	0.08428	1.21	0.84847	1.06	0.073	0.85	1298.9	23.4	623.8	4.9	454.2	3.8	73
11	441	277	0.63	0.06154	1.3	0.65029	1.16	0.07662	0.86	658.2	27.7	508.7	4.6	475.9	3.9	94
12	1181	1318	1.12	0.11264	1.07	1.25221	0.9	0.08061	0.84	1842.5	19.2	824.4	5.1	499.8	4.1	61
13	1724	1755	1.02	0.05708	1.07	0.6042	0.91	0.07675	0.85	494.2	23.8	479.9	3.5	476.7	3.9	99
14	372	242	0.65	0.05765	1.28	0.62097	1.14	0.0781	0.86	516.4	28.1	490.5	4.4	484.8	4	99
15	514	410	0.8	0.08606	1.38	0.89608	1.24	0.07551	0.89	1339.5	26.5	649.6	6	469.3	4	72
16	444	228	0.51	0.05759	1.27	0.65182	1.14	0.08209	0.86	513.7	27.3	509.6	4.6	508.6	4.2	99
17	357	224	0.63	0.05824	1.29	0.63918	1.15	0.07959	0.87	538.3	28.4	501.8	4.6	493.7	4.1	98
18	347	208	0.6	0.05848	1.3	0.63345	1.16	0.07856	0.87	547.6	28	498.2	4.6	487.5	4.1	98
KBY2-21 (Rhyolite)																
1	362	224	0.62	0.05992	1.97	0.64407	1.88	0.07795	0.97	600.6	42.2	504.8	7.5	483.9	4.6	96
2	451	368	0.82	0.05749	1.97	0.64395	1.87	0.08122	0.97	510.1	42.9	504.7	7.4	503.4	4.7	100
3	222	118	0.53	0.05851	2.58	0.64286	2.48	0.07967	1.05	548.8	55.2	504.1	9.9	494.2	5	98
4	338	261	0.77	0.06864	1.91	0.75834	1.82	0.08011	0.97	887.8	39.1	573.1	8	496.8	4.7	87
5	382	226	0.59	0.05951	1.9	0.64839	1.81	0.079	0.96	585.7	40.7	507.5	7.2	490.1	4.6	97
6	385	224	0.58	0.05827	1.96	0.63396	1.86	0.07888	0.96	539.1	42.8	498.6	7.3	489.4	4.6	98
7	239	132	0.55	0.05713	2.49	0.62742	2.39	0.07962	1.04	496	54.3	494.5	9.3	493.8	4.9	100
8	733	650	0.89	0.05734	1.95	0.63794	1.85	0.08066	0.97	504	42.7	501	7.3	500.1	4.7	100
9	512	429	0.84	0.05978	2.04	0.63892	1.94	0.07748	0.98	595	44.1	501.6	7.7	481.1	4.6	96
10	224	124	0.56	0.05891	2.41	0.65086	2.32	0.08009	1.02	563.6	51.8	509	9.3	496.7	4.9	98
11	453	302	0.67	0.05801	1.88	0.64417	1.79	0.08049	0.96	529.7	41.2	504.9	7.1	499	4.6	99
12	218	111	0.51	0.06141	3.13	0.65863	3.03	0.07773	1.16	653.6	65.9	513.8	12.2	482.6	5.4	94
13	319	170	0.53	0.05831	2.16	0.63962	2.07	0.0795	0.99	540.8	47.3	502.1	8.2	493.1	4.7	98
14	323	202	0.62	0.05942	2.22	0.65287	2.13	0.07963	1	582.5	47.7	510.2	8.6	493.9	4.8	97
15	163	77	0.47	0.05892	2.68	0.64418	2.58	0.07923	1.06	564.3	57.3	504.9	10.3	491.5	5	97
16	215	113	0.52	0.06393	4.61	0.68882	4.48	0.07809	1.46	739.2	94.7	532.1	18.6	484.7	6.8	91
17	362	191	0.53	0.06082	2.15	0.6626	2.05	0.07895	0.99	632.9	45.6	516.2	8.3	489.8	4.7	95
18	364	261	0.72	0.05963	2.77	0.66012	2.68	0.08022	1.07	590.3	59	514.7	10.8	497.4	5.2	97
19	277	249	0.9	0.07154	2.82	0.80392	2.71	0.08143	1.13	972.9	56.5	599	12.3	504.6	5.5	84
20	308	163	0.53	0.05811	2.24	0.64491	2.13	0.08041	0.99	533.6	48.6	505.3	8.5	498.6	4.8	99
21	158	77	0.49	0.06164	4.04	0.66688	3.92	0.07839	1.31	661.7	84.3	518.8	15.9	486.5	6.2	94
22	284	205	0.72	0.06081	2.02	0.67154	1.92	0.08002	0.97	632.4	42.9	521.6	7.8	496.3	4.6	95
1	429	400	0.93	0.0734	3.46	0.70984	3.15	0.07092	1.29	1024.995	70.4	544.653	13.3	441.6716	5.5	79
2	462	295	0.64	0.06083	1.64	0.65543	1.86	0.07804	0.82	633	67.6	511.8	7.5	484.4	3.8	94
3	678	504	0.74	0.06958	2.23	0.73254	2.3	0.07655	1.42	916.665	41.7	558.0407	9.9	475.5089	6.5	84
4	797	721	0.91	0.06306	1.59	0.66919	2.16	0.07669	1.2	709.3	33.3	520.2	8.8	476.4	5.5	91
5	645	586	0.91	0.05731	1.85	0.64567	2.09	0.08144	0.75	501.9	40.7	505.8	8.3	504.7	3.7	99
6	429	219	0.51	0.05785	2.49	0.63527	2.78	0.07934	0.92	524.1	55.5	499.4	11	492.2	4.4	98
7	273	193	0.71	0.06131	2.85	0.67439	2.94	0.07959	1.05	650	61.1	523.4	12	493.7	5	94
8	886	992	1.12	0.05668	1.68	0.63919	1.93	0.08145	0.95	479.7	37	501.8	7.7	504.8	4.6	99
9	495	394	0.79	0.06177	2.08	0.67643	2.18	0.07909	0.83	664.8	44.4	524.6	8.9	490.7	3.9	93
10	555	465	0.84	0.05645	1.89	0.62456	2.42	0.07966	1.11	477.8	47.2	492.7	9.5	494.1	5.3	99
11	587	350	0.6	0.06011	2.17	0.64512	2.51	0.07739	0.63	609.3	46.3	505.5	10	480.5	2.9	94
12	654	457	0.7	0.05693	2.55	0.61307	2.78	0.07787	0.92	487.1	55.6	485.5	10.7	483.4	4.3	99
13	291	177	0.61	0.05673	3.45	0.63346	3.65	0.08065	0.86	479.7	50	498.2	14.4	500	4.2	99
14	571	355	0.62	0.05802	2.19	0.64808	2.4	0.08079	1.1	531.5	46.3	507.3	9.6	500.8	5.3	98
15	542	359	0.66	0.05726	2.6	0.62954	2.46	0.07965	0.87	501.9	62	495.8	9.7	494	4.1	99

Table 3

Concentrations of major (wt%) and trace elements (ppm) of the volcanic rocks in southern Kaladawan district.

Sample No.	KFP-34	KFP-39	KFP-42	KFP-43	KFP-56	KFP-57	KFP-35	KFP-36	KFP-47	KFP-53	KLDB-V2	KWP-1	KWP-2	KBY2-21	KBY2-22	KLDB-V1
SiO ₂	57.84	58.75	55.84	60.66	53.72	52.37	70.86	67.00	71.12	74.23	64.46	65.9	78.55	72.62	76.82	67.73
TiO ₂	1.35	0.71	0.78	0.65	2.38	1.05	0.43	0.52	0.58	0.47	1.07	0.76	0.14	0.42	0.11	0.83
Al ₂ O ₃	15.54	15.43	14.97	16.12	13.83	14.62	13.23	13.61	12.5	10.83	14.24	12.58	9.13	13.8	10.19	14.59
MgO	2.06	4.39	10.41	2.03	2.71	10.97	2.51	3.72	2.16	2.13	2.23	1.87	1.21	0.84	0.36	1.28
Fe ₂ O _{3T}	8.22	8.27	8.63	9.31	14.92	12.17	3.87	6.00	4.26	3.61	8.06	9.86	4.35	3.05	3.71	4.10
MnO	0.17	0.11	0.07	0.07	0.22	0.14	0.04	0.06	0.03	0.03	0.28	0.07	0.04	0.11	0.01	0.07
CaO	3.04	4.87	1.25	3.25	5.51	1.52	2.43	2.74	2.21	1.46	0.91	0.57	0.05	0.12	0.06	0.25
Na ₂ O	6.07	3.25	1.49	3.62	3.82	0.91	3.39	2.86	2.98	2.28	5.80	5.35	0.35	5.55	2.23	4.95
K ₂ O	2.62	1.02	0.29	0.72	0.29	0.15	0.64	0.63	1.08	1.34	1.37	0.32	3.11	1.00	2.43	1.65
P ₂ O ₅	0.33	0.09	0.10	0.49	0.58	0.17	0.05	0.37	0.72	0.44	0.19	0.28	0.02	0.03	0.01	0.09
LOI	2.15	2.65	5.30	2.66	1.25	5.81	1.75	2.09	1.77	1.97	2.04	1.38	1.59	1.54	2.85	3.34
Total	99.51	99.64	99.19	99.62	99.27	99.90	99.24	99.66	99.44	98.82	99.39	99.03	98.87	99.1	98.84	98.93
Na ₂ O/K ₂ O	2.32	3.19	5.14	5.03	13.17	6.07	5.30	4.54	2.76	1.70	4.23	16.72	0.11	5.55	0.92	3.00
Na ₂ O + K ₂ O	8.69	4.27	1.78	4.34	4.11	1.06	4.03	3.49	4.06	3.62	7.17	5.67	3.46	6.55	4.66	6.60
A/CNK	1.32	1.69	4.94	2.12	1.44	5.67	2.05	2.18	1.99	2.13	1.76	2.02	2.60	2.07	2.16	2.13
Mg#	33	51	70	30	26	64	56	55	50	54	35	27	36	35	16	38
Sc	24.1	54.6	50.7	16.6	33.5	42.1	10.5	13.7	12.3	11.4	16.7	14.7	4.26	11.5	5.25	14.6
V	133	210	221	147	164	154	33	155	159	137	69.5	10.1	3.41	8.59	2.02	58.4
Cr	17.7	322	329	41.6	15.9	236	28.1	38.2	43.6	37.5	14.6	2.79	3.06	3.43	5.12	5.07
Co	12.1	12.1	11.2	6.5	3.74	1.89	1.52	15.5	1.15	15.3	17.5	19.9	12.7	26.1	23.9	9.31
Ni	7.04	6.05	5.48	44.6	6.51	7.84	12.2	93.6	53.7	60.0	26.3	2.20	2.30	3.01	3.08	4.10
Cu	22.3	6.55	23.3	5.16	33.6	7.64	6.51	6.97	17.7	45.4	11.4	13.5	3.30	43.1	40.0	27.0
Zn	215	58.4	113	86.6	142	141	34.8	47.7	66.7	57.8	349	39.3	112	222	113	209
Ga	23.8	15.4	18	18.2	24.8	18.7	14.2	17.9	14.3	13.6	17.4	23.6	14.6	17.9	17.9	24.2
Rb	70.1	59.6	21.8	38.6	8.86	9.18	42.3	37.9	42.3	62.7	3.55	12.1	68.6	44.1	38.5	73.2
Sr	148	377	119	319	273	94.4	323	297	157	131	91.1	127	65.5	70.6	56.9	131
Y	50.5	38.4	22.0	39.8	52.9	34.6	38.3	42.3	39.0	41.6	51.5	63.8	39.8	52.5	39.5	46.0
Zr	314	91.3	102	286	283	129	271	254	237	180	372	339	325	356	224	391
Nb	16.8	5.74	6.08	12.6	17.1	8.77	14.0	13.1	14.8	10.8	20.5	20.1	13.6	22.8	17.9	21.5
Cs	0.62	0.64	0.22	0.41	0.25	0.07	0.29	0.50	0.2	0.31	0.09	0.19	0.75	0.17	0.19	0.26
Ba	204	304	121	214	114	54.8	181	206	286	354	488	795	592	431	494	474
La	30.3	17.3	8.74	24.3	30.5	24.6	68.8	34.6	51.8	47.2	55.5	71.5	27.4	28.1	27.9	32.1
Ce	64.2	31.0	18.0	15.0	65.1	40.3	145	67.4	83.2	81.	110	141	59.6	44.8	43.5	48.4
Pr	8.29	3.85	1.86	6.34	8.94	5.26	15.5	9.69	10.8	11.9	12.7	17.0	7.21	5.79	1.27	6.23
Nd	32.4	14.8	7.07	26.5	37.5	19.8	56.0	36.8	39.3	45.6	46.7	66.9	27.1	21.7	4.96	23.3
Sm	7.95	3.91	1.51	6.66	9.24	4.62	11.0	7.88	7.59	9.21	9.97	14.1	5.61	4.95	1.72	5.46
Eu	1.87	0.67	0.30	1.83	2.48	0.73	1.22	1.32	1.15	1.39	2.22	2.98	0.63	0.50	0.23	0.98
Gd	9.07	5.05	1.85	7.21	10.92	5.17	9.38	7.45	6.90	8.75	10.11	13.51	5.80	5.88	3.53	6.30
Tb	1.51	0.91	0.35	1.20	1.73	0.87	1.45	1.27	1.14	1.37	1.76	2.24	1.07	1.16	0.84	1.22
Dy	9.31	6.14	2.61	7.39	10.3	5.38	7.66	7.27	6.63	7.66	10.5	12.6	6.98	8.66	6.60	8.40
Ho	1.95	1.34	0.67	1.60	2.14	1.16	1.46	1.50	1.40	1.54	2.17	2.63	1.63	2.05	1.58	1.88
Er	5.78	3.95	2.29	4.87	6.22	3.49	4.34	4.54	4.34	4.62	6.37	7.68	5.18	6.47	5.00	5.90
Tm	0.85	0.61	0.37	0.76	0.89	0.53	0.63	0.67	0.66	0.66	0.91	1.10	0.81	1.01	0.78	0.92
Yb	5.44	4.03	2.58	5.12	5.67	3.49	4.29	4.48	4.56	4.29	5.90	7.05	5.29	6.57	5.13	6.16
Lu	0.78	0.55	0.41	0.79	0.85	0.55	0.62	0.67	0.73	0.65	0.86	1.06	0.77	0.98	0.71	0.93
Hf	8.03	2.50	2.70	7.95	6.87	3.45	7.99	6.48	6.41	4.68	9.58	9.74	7.72	10.8	6.57	9.89
Ta	1.71	0.53	0.47	0.81	1.11	0.62	1.09	1.91	1.70	0.68	1.23	1.34	0.32	1.23	0.87	1.09
Tl	0.44	0.32	0.10	0.24	0.06	0.04	0.20	0.20	0.17	0.30	0.03	0.06	0.44	0.27	0.49	1.01
Pb	24.1	15.3	7.01	165	11.8	6.05	9.05	31.2	13.6	11.4	30.9	10.7	13.5	20.1	25.5	29.9
Th	11.5	4.38	4.71	1.56	8.96	6.19	13.2	11.6	11.7	9.78	18.9	14.6	11.8	19.6	13.5	16.3
U	3.74	2.35	2.56	1.83	5.34	2.21	3.55	4.73	8.00	6.96	4.51	5.49	3.15	8.71	5.08	8.93
Sr/Y	2.9	9.8	5.4	8.0	5.2	2.7	8.4	7.0	4.0	3.1	1.8	2.0	1.6	1.3	1.4	2.8
Nb/Ta	9.8	10.8	12.9	15.6	15.4	14.1	12.8	6.9	8.7	15.9	16.7	15.0	42.5	18.5	20.6	19.7
Zr/Hf	39.1	36.5	37.8	36.0	41.2	37.4	33.9	39.2	37.0	38.5	38.8	34.8	42.1	33.0	34.1	39.5
Yb _N	32.0	23.7	15.2	30.1	33.4	20.5	25.2	26.4	26.8	25.2	34.7	41.5	31.1	38.6	30.2	36.2
(La/Yb) _N	4.0	3.1	2.4	3.4	3.9	5.1	11.5	5.5	8.1	7.9	6.7	7.3	3.7	3.1	3.9	3.7

$$\text{Mg\#} = (\text{MgO}/40.31)/(\text{MgO}/40.31 + \text{Fe}_2\text{O}_{3T} * 0.8998/71.85 * 0.85) * 100;$$

Normalization values of rare earth elements are from Sun and McDonough (1989).

(2SD) ($n = 16$), and $^{207}\text{Pb}/^{206}\text{Pb} = 0.91443 \pm 0.00001$ (2SD) ($n = 16$), consistent with the values measured by Platzner et al. (2001).

4.4. Zircon Hf isotopes

Zircon Hf isotope analysis was carried out in-situ using a Resolution M-50 laser-ablation microprobe, attached to a Neptune Plus MC-ICP-MS at the State Key Laboratory of Isotope Geochemistry, GIGCAS. Instrumental conditions and data acquisition were described by Wu et al. (2006). A stationary spot was used for the analysis, with a beam diameter of 45 μm and He and Ar as carrier gases. To correct the isobaric interferences of ^{176}Lu and ^{176}Yb on ^{176}Hf , appropriate $^{176}\text{Lu}/^{175}\text{Lu}$ and $^{176}\text{Yb}/^{172}\text{Yb}$ ratios were

determined, respectively (Wu et al., 2006). The zircon standard Penglai was used and yielded a weighted mean $^{176}\text{Hf}/^{177}\text{Hf}$ ratio of 0.282879 ± 15 (2 σ), consistent with the value of 0.282906 ± 10 obtained by X.H. Li et al. (2010).

5. Results

5.1. Zircon age

The zircons (50–200 μm long with aspect ratios of 1:1 to 2:1) are colorless, transparent, prismatic and euhedral, and display oscillatory zoning (Fig. 7). The 18 zircons analyzed contain U and Th

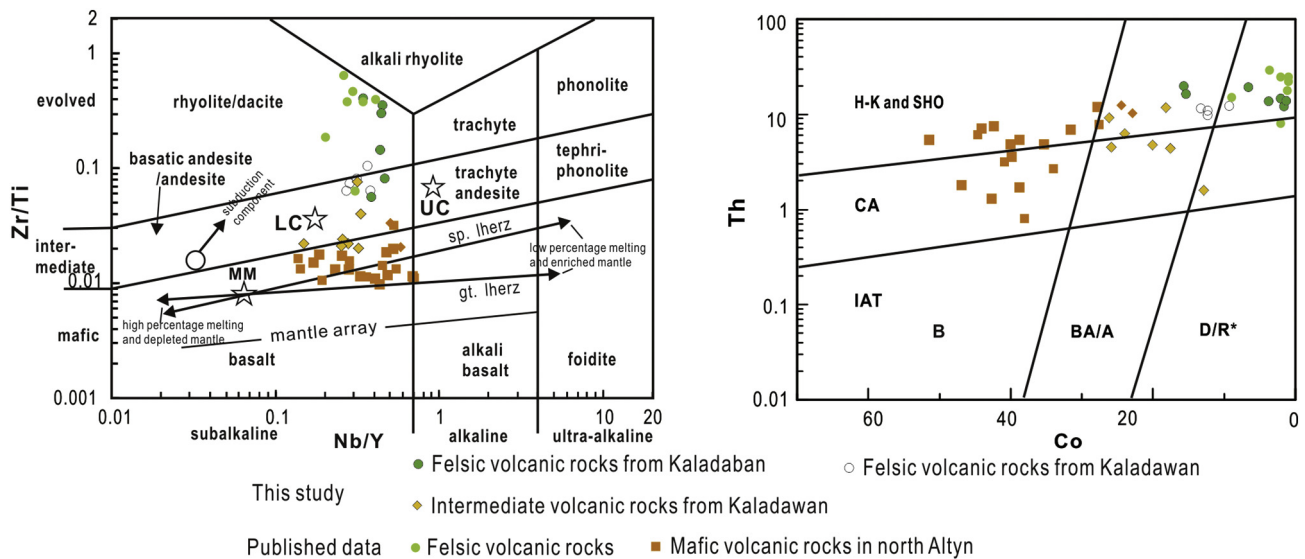


Fig. 8. Geochemical discrimination diagrams for the volcanic rocks in the southern Kaladawan district: (a) Nb/Y vs. Zr/Ti (Pearce, 1996; Winchester and Floyd, 1977). (b) Co-Th (Hastie et al., 2007). LC—lower crust; UC—upper crust; MM—MORB mantle; sp.lherz—spinel lherzolite; gt.lherz—garnet lherzolite. IAT—Island arc tholeiite; CA—Calc-alkaline; H—K and SHO—High-K calc-alkaline and shoshonite; B—Basalt, BA/A—Basaltic andesite/andesite; D/R*—Dacite/rhyolite. Data for volcanic rocks in the northern Altyn are from Cui et al. (2010) and Li et al. (2013). Data for the LC, MC, and UC compositions are from Rudnick and Gao (2003).

concentrations of 133–1724 ppm and 51–1755 ppm, respectively, with Th/U ratios of 0.38–1.12 (Table 2). After discarding four zircons with low concordance (<90%), 14 zircons yielded a weighted mean $^{206}\text{U}/^{238}\text{Pb}$ age of 490.5 ± 5.2 Ma (MSWD = 6.2) (Fig. 7a), representing the eruptive age of the Kaladawan intermediate volcanic rocks.

5.1.2. KBY2-21 (rhyolite)

The zircons (100–200 μm long with aspect ratios of 1:1 to 3:1) are colorless, transparent, elongated, prismatic and euhedral, and display

regular oscillatory zoning (Fig. 7). The 22 zircons analyzed contain U and Th concentrations of 158–733 ppm, 78–650 ppm, respectively, with Th/U ratios of 0.35–0.82 (Table 2). After discarding two zircons with low concordance (<90%), 20 zircons yielded a weighted mean $^{206}\text{U}/^{238}\text{Pb}$ age of 492.6 ± 2.9 Ma (MSWD = 1.6) (Fig. 7b).

5.1.3. KBY2-22 (rhyolite)

Zircon grains of the sample are colorless to light green, transparent and euhedral in shape, and also display regular oscillatory

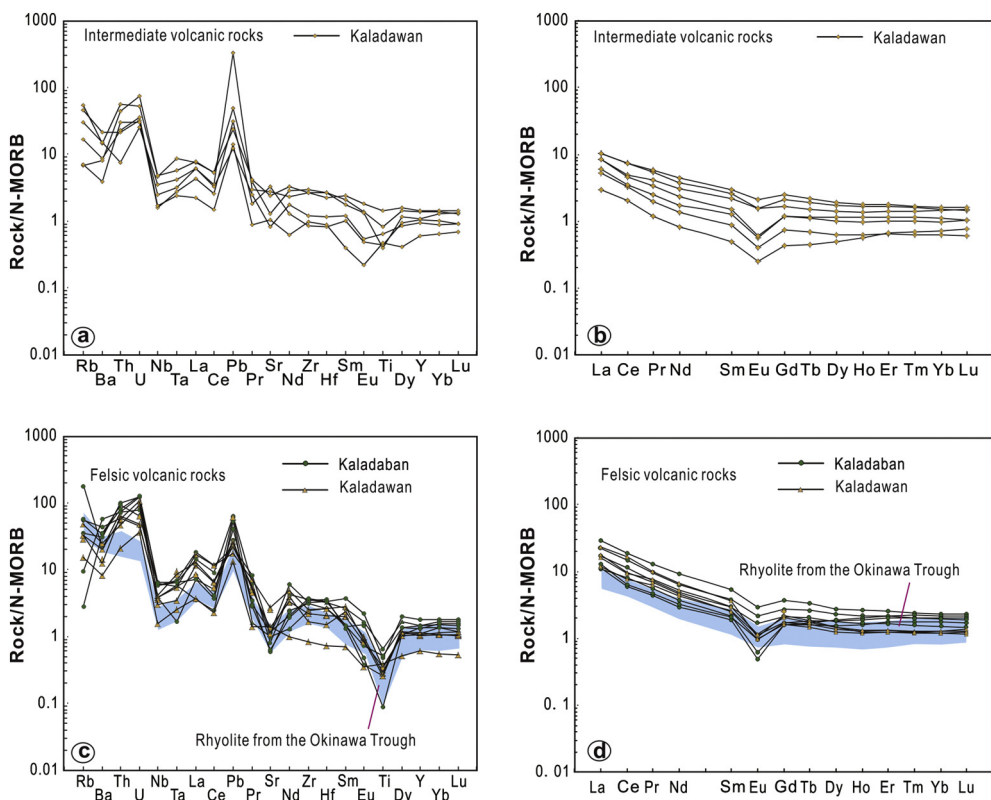


Fig. 9. N-MORB-normalized (a, c) multi-element and (b, d) REE patterns the volcanic rocks in the southern Kaladawan district. Data for N-MORB and the Okinawa Trough rhyolite are from Hofmann (1988) and Shinjo and Kato (2000), respectively.

Table 4

Sr and Nd isotope compositions of the volcanic rocks in southern Kaladawan district.

Sample number	Rb (ppm)	Sr (ppm)	Rb/Sr	$^{87}\text{Sr}/^{86}\text{Sr}$	σ	$^{87}\text{Rb}/^{86}\text{Sr}$	$(^{87}\text{Sr}/^{86}\text{Sr})_i$	Sm (ppm)	Nd (ppm)	Sm/Nd	$^{143}\text{Nd}/^{144}\text{Nd}$	σ	$^{147}\text{Sm}/^{144}\text{Nd}$	$(^{143}\text{Nd}/^{144}\text{Nd})_i$	ϵ_{Nd}	$T_{\text{DM}1}$ (Ga)	$T_{\text{DM}2}$ (Ga)
Andesite																	
KFP-39	59.6	377	0.16	0.71152	6	0.46	0.7083	3.91	14.8	0.26	0.512051	4	0.16	0.511519	-9.4	3.1	2
KFP-43	38.6	319	0.12	0.71067	5	0.35	0.7082	6.66	26.5	0.25	0.51212	6	0.16	0.511614	-7.6	2.5	1.8
Rhyolite																	
KBY2-21	44.1	70.6	0.62	0.71904	6	1.81	0.7063	4.95	21.7	0.23	0.512271	4	0.14	0.511812	-3.7	1.7	1.5
KBY2-22	38.5	56.9	0.68	0.72136	6	1.96	0.7076	1.72	4.96	0.35	0.512364	4	0.22	0.511667	-6.6	2.7	1.7
KLDB-V1	73.2	131	0.56	0.71821	6	1.62	0.7068	5.46	23.3	0.23	0.512331	3	0.15	0.511859	-2.8	1.7	1.4
KLDB-V2	3.55	91.1	0.04	0.71026	8	0.11	0.7095	9.97	46.7	0.21	0.512356	3	0.13	0.511927	-1.5	1.4	1.3
KFP-36	37.9	297	0.13	0.7121	6	0.37	0.7095	7.88	36.8	0.21	0.511938	3	0.13	0.511508	-9.7	2.1	2

$^{87}\text{Sr}/^{86}\text{Sr}$ ratio was calculated using $\lambda_{\text{Rb}} = 1.42 \times 10^{-11} \text{ a}^{-1}$ (Steiger and Jäger, 1977). Reference constants used in $\epsilon_{\text{Nd}}(t)$ and T_{DM} calculations include $(^{147}\text{Sm}/^{144}\text{Nd})_{\text{CHUR}} = 0.1967$, $(^{143}\text{Nd}/^{144}\text{Nd})_{\text{CHUR}} = 0.512638$ (Jacobsen and Wasserburg, 1980), $(^{147}\text{Sm}/^{144}\text{Nd})_{\text{DM}} = 0.2137$ and $(^{143}\text{Nd}/^{144}\text{Nd})_{\text{DM}} = 0.51315$ (Peucat et al., 1989).

zoning, with lengths of 100–200 μm and aspect ratios of 1:1 to 3:1. Twenty zircons analyzed contain U and Th concentrations of 273–886 ppm, 177–992 ppm, respectively, with Th/U ratios of 0.51–1.12. After discarding two zircons with low concordance (<90%), 13 zircons yielded a weighted mean $^{206}\text{U}/^{238}\text{Pb}$ age of 491.6 ± 5.6 Ma (MSWD = 4.8) (Fig. 7c).

5.2. Whole-rock geochemistry and isotopes

5.2.1. Major oxides

5.2.1.1. Intermediate volcanic rocks. Six samples analyzed contain high LOI (1.25–5.81%). They have $\text{SiO}_2 = 52.37\text{--}60.66$ wt%, $(\text{Na}_2\text{O} + \text{K}_2\text{O}) = 1.06\text{--}8.69$ wt%, $\text{Al}_2\text{O}_3 = 13.83\text{--}16.12$ wt%, and $\text{CaO} = 1.25\text{--}5.51$ wt%. The samples are characterized by high and varying A/CNK ratios (1.05–5.67) (Table 3).

5.2.1.2. Felsic volcanic rocks. Four rhyolite samples from the Kaladawan area contain SiO_2 (67.00–74.23 wt%), TiO_2 (0.43–0.58 wt%), Al_2O_3 (10.83–13.61 wt%), Fe_2O_3 (3.61–6.00 wt%), MgO (2.13–3.72 wt%), CaO (1.46–2.74 wt%), Na_2O (2.28–3.39 wt%), K_2O (0.63–1.34 wt%), and P_2O_5 (0.05–0.72 wt%). These samples are characterized by high A/CNK ratios (1.99–2.18) and high Mg# values (51–56). The felsic volcanic rocks from the Kaladaban Zn–Pb deposit have varying contents of SiO_2 (64.46–78.55 wt%), TiO_2 (0.11–1.07 wt%), Al_2O_3 (9.13–14.59 wt%), Fe_2O_3 (3.05–9.86 wt%), MgO (0.36–2.23 wt%), CaO (0.06–0.91 wt%), Na_2O (0.35–5.80 wt%), K_2O (0.32–3.11 wt%), and P_2O_5 (0.01–0.27 wt%). These rocks are characterized by high A/CNK ratios (1.76–2.60) and low Mg# values (16–38) (Table 3).

5.2.2. Trace elements

5.2.2.1. Intermediate volcanic rocks. The samples plot in the basaltic-andesite and andesite fields (Fig. 8a) and are high-K calc-alkaline and shoshonitic (Fig. 8b). They are enriched in large ion lithophile elements (LILEs: Rb, U, Th and Pb) and depleted in high field strength elements (HFSEs: Nb, Ta and Ti) (Fig. 9a), and have

high Th/Y ratios (1.1–3.2). The rocks contain Sr and Y concentrations of 94.4–377 ppm and 22.0–52.9 ppm, respectively, giving Sr/Y ratios of 2.7–9.8. In the N-MORB-normalized REE diagram, all samples have no or slight LREE/HREE enrichment with distinct (to moderately distinct) negative Eu anomalies (Fig. 9b). They contain total REE concentrations ($\sum\text{REE}$) of 49–193 ppm, with LREE/HREE ratios of 3.2–4.7, $(\text{La}/\text{Yb})_N$ ratios of 4.1–8.6, and δEu of 0.50–0.80 (Table 3).

5.2.2.2. Felsic volcanic rocks. Samples from the Kaladawan area and the Kaladaban Zn–Pb deposit have similar trace element features. Most samples plot in the dacite and rhyolite fields (Fig. 8a) and are high-K calc-alkaline and shoshonitic (Fig. 8b). Most samples are highly enriched in LILEs and depleted in HFSEs, and contain slight LREE/HREE enrichment with obvious negative Eu anomalies (Fig. 9c, d). They have low Sr (56.9–323 ppm) and high Y (38.3–63.8 ppm) concentrations, yielding low Sr/Y ratios (1.3–8.4). These rocks contain $\sum\text{REE}$ of 103–361 ppm, LREE / HREE ratios of 1.2–10.0, $(\text{La}/\text{Yb})_N$ ratios of 3.3–19.6, and δEu of 0.28–0.67. Notably, the samples from the Kaladaban Zn–Pb deposit have higher Sr/Y, LREE/HREE and $(\text{La}/\text{Yb})_N$ ratios than those of from the Kaladawan area (Table 3).

5.2.3. Sr–Nd–Pb isotopes

5.2.3.1. Intermediate volcanic rocks. The samples yield $(^{87}\text{Sr}/^{86}\text{Sr})_i$ values of 0.7082–0.7083 and $\epsilon_{\text{Nd}}(t)$ values of -9.4 to -7.6, with two-stages model ages of 2.0–1.8 Ga. The samples also have high initial $^{206}\text{Pb}/^{204}\text{Pb}$ ratios (18.431–18.872), $^{207}\text{Pb}/^{204}\text{Pb}$ ratios (15.623–15.646), and $^{207}\text{Pb}/^{204}\text{Pb}$ ratios (37.978–38.309).

5.2.3.2. Felsic volcanic rocks. As shown in Tables 4 and 5, the samples are characterized by $(^{87}\text{Sr}/^{86}\text{Sr})_i$ values of 0.7063–0.7095. They also have $\epsilon_{\text{Nd}}(t)$ values ranging from -9.7 to -1.5, with two-stages model ages of 2.0–1.3 Ga. Moreover, they have high radiogenic Pb isotopic composition, with present whole-rock $^{206}\text{Pb}/^{204}\text{Pb}$, $^{207}\text{Pb}/^{204}\text{Pb}$ and $^{207}\text{Pb}/^{204}\text{Pb}$ ratios of 19.024–21.582,

Table 5

Lead isotope compositions of the volcanic rocks in southern Kaladawan district.

Sample number	U (ppm)	Th (ppm)	Pb (ppm)	$^{206}\text{Pb}/^{204}\text{Pb}$	σ	$^{207}\text{Pb}/^{204}\text{Pb}$	σ	$^{208}\text{Pb}/^{204}\text{Pb}$	σ	$(^{206}\text{Pb}/^{204}\text{Pb})_i$	$(^{207}\text{Pb}/^{204}\text{Pb})_i$	$(^{208}\text{Pb}/^{204}\text{Pb})_i$
Andesite												
KFP-39	2.35	4.38	15.3	19.665	3	15.6909	2	38.7831	10	18.872	15.646	38.309
KFP-43	1.83	1.56	165	18.4865	2	15.6267	2	37.993	8	18.431	15.623	37.978
Rhyolite												
KBY2-21	8.71	19.6	20.1	21.5823	3	15.8014	3	40.3548	17	19.237	15.668	38.661
KBY2-22	5.08	13.5	25.5	19.0243	3	15.6558	2	38.7933	12	18.004	15.598	37.923
KLDB-V1	8.93	16.3	29.9	20.724	3	15.7533	2	40.3228	11	19.127	15.662	39.387
KLDB-V2	4.51	18.9	30.9	20.6018	3	15.7447	3	40.4146	12	19.822	15.7	39.365
KFP-36	4.73	11.6	31.2	19.5631	3	15.6905	3	38.5223	9	18.784	15.646	37.909

Table 6

Lu–Hf isotope compositions of the volcanic rocks in southern Kaladawan district.

Sample number	Age(Ma)	$^{176}\text{Yb}/^{177}\text{Hf}$	$^{176}\text{Lu}/^{177}\text{Hf}$	$^{176}\text{Hf}/^{177}\text{Hf}$	2σ	$(^{176}\text{Hf}/^{177}\text{Hf})_i$	$\epsilon_{\text{Hf}}(0)$	$\epsilon_{\text{Hf}}(t)$	$T_{\text{DM}, 1}(\text{Ga})$	$T_{\text{DM}, 2}(\text{Ga})$	$f_{(\text{Lu/Hf})}$
KFP-43											
1	496.4	0.06457	0.001722	0.2826	0.000016	0.282584	-6.1	4.3	0.94	1.19	-0.95
2	500.2	0.095886	0.002552	0.282646	0.000014	0.282622	-4.5	5.7	0.9	1.1	-0.92
7	495.3	0.060749	0.001658	0.282604	0.000014	0.282589	-5.9	4.4	0.93	1.18	-0.95
11	482.6	0.064611	0.001699	0.282602	0.000014	0.282586	-6	4.1	0.94	1.2	-0.95
14	478.4	0.052438	0.001474	0.282654	0.000014	0.28264	-4.2	5.9	0.86	1.08	-0.96
16	484.8	0.071862	0.002231	0.282567	0.000015	0.282546	-7.3	2.7	1.00	1.28	-0.93
21	508.6	0.055791	0.001513	0.28256	0.000012	0.282545	-7.5	3.2	0.99	1.27	-0.95
KBY2-21											
3	494.2	0.086926	0.002218	0.28255	0.000012	0.282529	-7.8	2.3	1.03	1.32	-0.93
6	496.8	0.049329	0.00148	0.28235	0.000015	0.282336	-14.9	-4.5	1.29	1.75	-0.96
7	490.1	0.061632	0.001572	0.282559	0.000013	0.282545	-7.5	2.8	1	1.28	-0.95
8	489.4	0.084707	0.00217	0.282587	0.000013	0.282567	-6.5	3.5	0.97	1.23	-0.93
9	493.8	0.085262	0.002278	0.282551	0.000015	0.28253	-7.8	2.3	1.03	1.31	-0.93
10	500.1	0.135758	0.003463	0.282545	0.000016	0.282512	-8	1.8	1.07	1.35	-0.9
12	496.7	0.060741	0.001629	0.282579	0.000014	0.282564	-6.8	3.6	0.97	1.24	-0.95
13	499	0.095881	0.002531	0.282517	0.000016	0.282494	-9	1.1	1.08	1.39	-0.92
15	493.1	0.071276	0.001882	0.282559	0.000015	0.282541	-7.5	2.7	1.01	1.29	-0.94
17	491.5	0.083252	0.00217	0.28256	0.000015	0.28254	-7.5	2.6	1.01	1.29	-0.93
20	497.4	0.067409	0.001861	0.282515	0.000015	0.282497	-9.1	1.2	1.07	1.39	-0.94
23	486.5	0.088668	0.002325	0.282501	0.000014	0.282479	-9.6	0.4	1.1	1.43	-0.93
24	496.3	0.059146	0.001558	0.282591	0.000014	0.282576	-6.4	4	0.95	1.21	-0.95
KBY2-22											
6	476.4	0.12413	0.003202	0.282569	0.000013	0.28254	-7.2	2.3	1.03	1.3	-0.9
8	492.2	0.064036	0.002054	0.282518	0.000022	0.282499	-9	1.2	1.07	1.38	-0.94
10	493.7	0.056095	0.001584	0.282322	0.000013	0.282307	-15.9	-5.6	1.34	1.81	-0.95
11	504.8	0.07214	0.001878	0.282557	0.000013	0.282539	-7.6	2.9	1.01	1.29	-0.94
15	494.1	0.076372	0.002358	0.282484	0.000031	0.282462	-10.2	-0.1	1.13	1.47	-0.93
17	480.5	0.069322	0.002037	0.282419	0.00002	0.282401	-12.5	-2.5	1.21	1.61	-0.94
19	500	0.05459	0.001388	0.282621	0.000014	0.282608	-5.4	5.2	0.9	1.14	-0.96
20	513.7	0.097175	0.002538	0.282484	0.000017	0.28246	-10.2	0.3	1.13	1.46	-0.92
21	500.8	0.090524	0.002611	0.282462	0.000018	0.282438	-11	-0.8	1.17	1.52	-0.92
22	494	0.090324	0.002842	0.282426	0.000023	0.2824	-12.2	-2.3	1.23	1.6	-0.91

15.656–15.801 and 38.522–40.415, respectively, and recalculated initial $^{206}\text{Pb}/^{204}\text{Pb}$, $^{207}\text{Pb}/^{204}\text{Pb}$ and $^{207}\text{Pb}/^{204}\text{Pb}$ ratios of 18.004–19.822, 15.598–15.700 and 37.923–39.387, respectively.

5.3. Zircon Hf isotopes

The decay constant for ^{176}Lu was set at $1.865 \times 10^{-11} \text{ year}^{-1}$ (Scherer et al., 2001). Initial $^{176}\text{Hf}/^{177}\text{Hf}$ ratios and $\epsilon_{\text{Hf}}(t)$ were calculated with the reference to the chondritic reservoir (CHUR) at

the time of zircon growth, the chondritic $^{176}\text{Hf}/^{177}\text{Hf}$ ratio (0.282772) and $^{176}\text{Lu}/^{177}\text{Hf}$ ratio (0.0332) are from Blichert-Toft and Albarède (1997). Single-stage model ages ($T_{\text{DM}1}$) were calculated with reference to the depleted mantle at the present-day $^{176}\text{Hf}/^{177}\text{Hf}$ ratio (0.28325), similar to that of the average MORB (Nowell et al., 1998) and $^{176}\text{Lu}/^{177}\text{Hf} = 0.0384$ (Griffin et al., 2000). Two-stage model ages ($T_{\text{DM}2}$) were calculated assuming a $^{176}\text{Lu}/^{177}\text{Hf} = 0.015$ for the average continental crust (Griffin et al., 2002). Errors in both $\epsilon_{\text{Hf}}(t)$ and T_{DM} were calculated based on the analytical errors alone, but

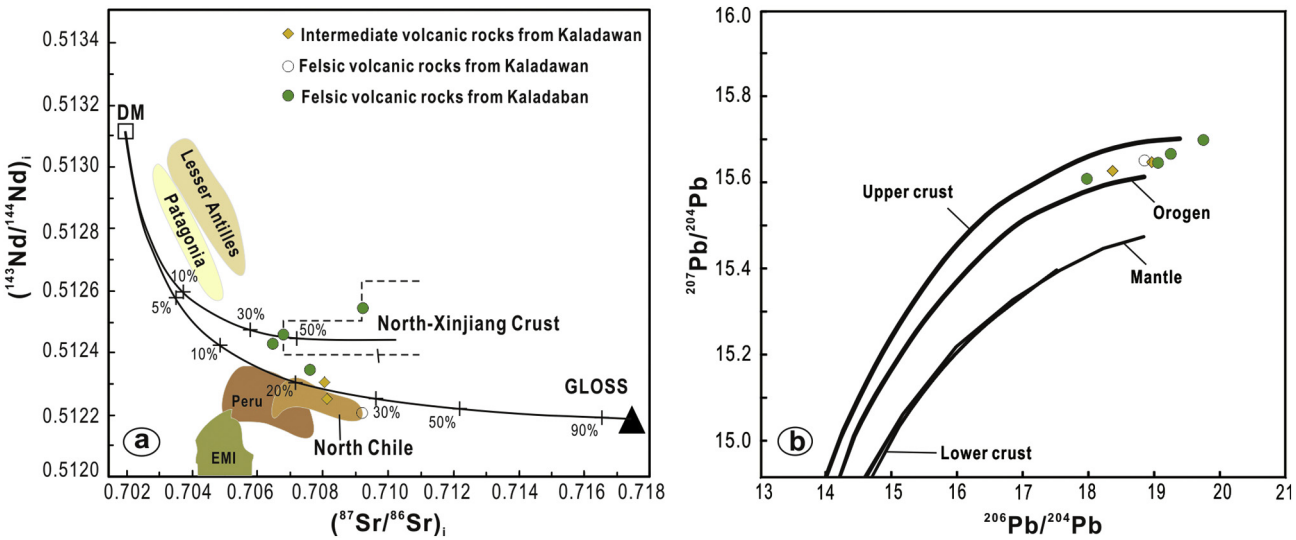


Fig. 10. Binary diagrams of (a) $(^{87}\text{Sr}/^{86}\text{Sr})_i$ vs. $(^{143}\text{Nd}/^{144}\text{Nd})_i$ (after Faure, 1977) and (b) $^{206}\text{Pb}/^{204}\text{Pb}$ vs. $^{207}\text{Pb}/^{204}\text{Pb}$ (after Zartman and Doe, 1981) for the volcanic rocks in the southern Kaladawan district. Data source: DM from Salters and Stracke (2004); global subducting sediment (GLOSS) from Plank and Langmuir (1998); and average crust of the Northern Xijiang from Zhu et al. (2001).

much bigger and poorly constrained errors could be associated with model Hf ages because of the errors with the reference model (Zheng et al., 2005).

Magmatic zircons from sample KFP-43 yielded $^{176}\text{Lu}/^{177}\text{Hf}$ ratios of 0.001474–0.002572, $^{176}\text{Hf}/^{177}\text{Hf}$ ratios of 0.282560–0.282654, $\epsilon_{\text{Hf}}(t)$ values of 2.7–5.9, T_{DM2} ages of 1.28 to 1.08 Ga and $f_{\text{Lu/Hf}}$ of −0.96 to −0.92.

Zircons from sample KBY2-21 contain $^{176}\text{Lu}/^{177}\text{Hf}$ and $^{176}\text{Hf}/^{177}\text{Hf}$ ratios of 0.001480–0.003463 and 0.282350–0.282591, respectively. The calculated $\epsilon_{\text{Hf}}(t)$ values = −4.5 to 4.0 (averaging 1.8), $f_{\text{Lu/Hf}} = -0.95$ to −0.90, and T_{DM2} ages = 1.75 to 1.21 Ga. Zircons from sample KBY2-22 contain $^{176}\text{Lu}/^{177}\text{Hf} = 0.001388–0.003202$, $^{176}\text{Hf}/^{177}\text{Hf} = 0.282322–0.282621$, $\epsilon_{\text{Hf}}(t) = -5.6$ to 5.2 (averaging 0.1), and $f_{\text{Lu/Hf}} = -0.96$ to −0.90. T_{DM2} ages are 1.81 to 1.14 Ga (Table 6).

6. Discussion

6.1. Ages of the VMS ore-hosting rocks in the southern Kaladawan district

VMS deposits in the northeastern Altyn Mountains, e.g., the Kaladaban Zn–Pb, Kaladabanxi Zn–Pb and Kaladawan Cu–Zn–Pb deposits, are hosted by the Kaladawan Formation felsic volcanic rocks. Previous studies proposed that these deposits are syngenetic, VMS-type based on their ore deposit geology (e.g., stratiform ore-bodies, lithological control on mineralization, laminated and banded ores) and geochemical features (e.g., Co–Ni contents of pyrite and S–Pb-isotope signatures, Cui, 2010). In this study, two volcanic ore hosts from the Kaladaban yielded similar late Cambrian zircon U–Pb ages of 492.6 ± 2.9 Ma and 491.6 ± 5.6 Ma, which represent the eruption age of these volcanic rocks and the primary VMS mineralization age in the Kaladawan district.

6.2. Petrogenesis of the volcanic rocks in the southern Kaladawan district

6.2.1. Intermediate volcanic rocks

The intermediate volcanic rocks comprise basaltic andesite and andesite and belong to high-K calc-alkaline and shoshonitic series (Fig. 8). They are characterized by high LILE and LREE enrichments and HFSE depletions (Fig. 9a, b), displaying arc geochemical affinities.

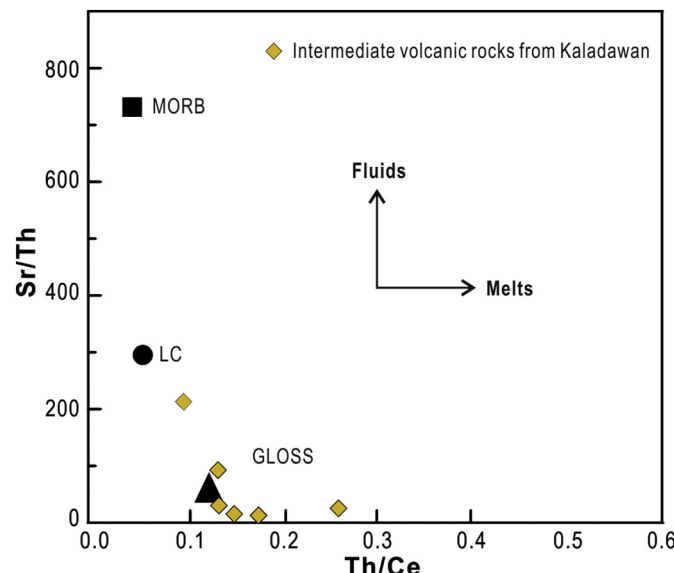


Fig. 11. Plot of Th/Ce vs. Sr/Th for the Kaladawan intermediate volcanic rocks.

These affinities were commonly interpreted to be caused by the metasomatism of oceanic slab-derived fluids to the lithosphere mantle in subduction-related environments (e.g., Harmon et al., 1981; Thorpe et al., 1979; Raymond, 1995; Ulmer, 2001; Zheng et al., 2015). The high $(^{87}\text{Sr}/^{86}\text{Sr})_i$ values (0.7082–0.7083; Fig. 10a) and radiogenic Pb isotope compositions (Fig. 10b) but low $\epsilon_{\text{Nd}}(t)$ values (−9.7 to −7.6) suggest an enriched mantle source (Zindler and Hart, 1986). Furthermore, the high Th contents, Th/Ce ratios (0.10–0.26; Fig. 11) and low Sr/Th ratios (13–86) indicate that the mantle was enriched by subducted sediments (Class et al., 2000; Hawkesworth et al., 1993; Plank and Langmuir, 1993; Raymond, 1995). Petrogenetic modeling was undertaken to test this hypothesis, using the values of depleted mantle (DM) to represent the mantle source and the global subducting sediments (GLOSS) to represent the sediments. Based on these starting materials, the Sr and Nd isotopic data show that these intermediate volcanic rocks could be generated by a mixture ratio (DM melt to GLOSS melt) of about 75:25 (Fig. 10a). Notably, these rocks show positive zircon $\epsilon_{\text{Hf}}(t)$ values (2.7–5.9, Fig. 12) and negative corresponding whole-rock $\epsilon_{\text{Nd}}(t)$ values (−9.4 to −7.6), indicating decoupled Hf–Nd isotope compositions (Chauvel et al., 2008; Vervoort and Blichert-Toft, 1999). Chauvel et al. (2008) proposed that higher proportions of pelagic sediments relative to terrigenous clasts in sourced subducting sediments could result in Hf–Nd isotopic decoupling. Higher solubility of Nd than Hf in the slab-derived fluids (Kessel et al., 2005; Polat and Münker, 2004; Vervoort et al., 1999; Woodhead et al., 2001), minor crustal contamination and/or hydrothermal alterations after zircon crystallization in the shallow crusts may also have contributed to the isotopic decoupling (Farmer and DePaolo, 1987). In brief, these intermediate volcanic rocks were likely produced by the partial melting of the mantle wedge enriched by subducted sediment inputs, in response to the introduction of fluids released from the subducted slabs.

6.2.2. Felsic volcanic rocks

Felsic volcanic rocks from the Kaladawan area and the Kaladaban Zn–Pb deposit have different geochemical characters and thus different petrogenetic signatures. Felsic volcanic rocks from the Kaladawan area shows a fractionation relationship with the Kaladawan intermediate volcanic rocks in terms of their major element variations: Decreasing Al_2O_3 , Fe_2O_3 , CaO , MgO , TiO_2 and MgO with increasing SiO_2 (Fig. 13). Both the felsic and intermediate rocks from the Kaladawan area have similar N-MORB-normalized trace element and REE patterns and whole-rock Sr, Nd, Hf, Pb isotope compositions (Figs. 10, 11), indicating that they were probably co-

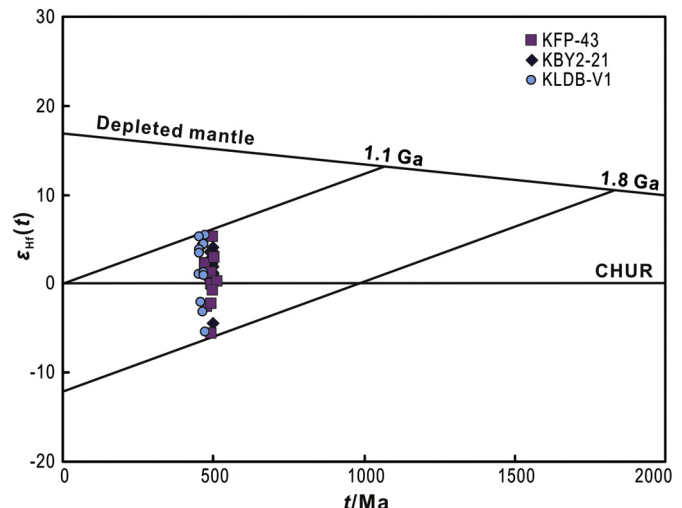


Fig. 12. Plot of zircon $\epsilon_{\text{Hf}}(t)$ vs. U–Pb age for the zircons from samples KBY2-21, KLDB-V1 and KFP-43.

magma (Mo et al., 2007). The fractionation relationship is also evident in the La vs. La/Yb diagram (Fig. 14).

The Kaladawan felsic volcanic rocks have high SiO₂ (64.46–78.55 wt%) and A/CNK ratios (1.76–2.60) and low TiO₂ (0.11–1.07 wt%), all of which indicate a highly evolved and strongly peraluminous nature, and suggest a likely crustal source. The geochemical trend in the La vs. La/Yb diagram also indicates that

the rocks were probably formed by partial melting rather than fractional crystallization (Fig. 14). The LILE enrichments and high Rb/Sr values suggest that these felsic volcanic rocks were probably derived from the partial melting of continental crust. In the ²⁰⁶Pb/²⁰⁴Pb vs. ²⁰⁷Pb/²⁰⁴Pb diagram (Fig. 10b), the samples plot between the orogen and upper crust evolution lines, suggesting an old Pb source (Zartman and Doe, 1981). The positive average zircon

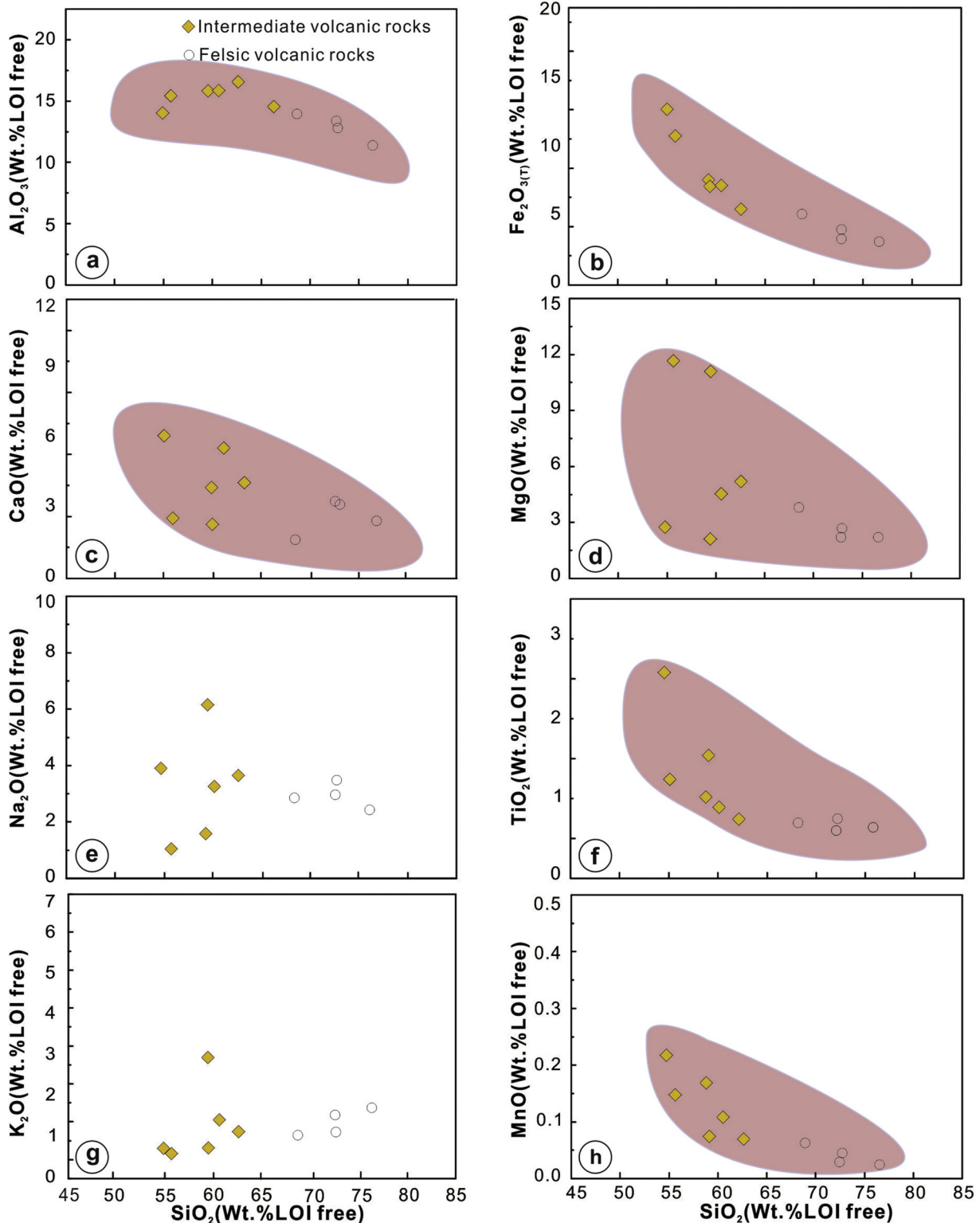


Fig. 13. Harker variation diagrams for the Kaladawan volcanic rocks.

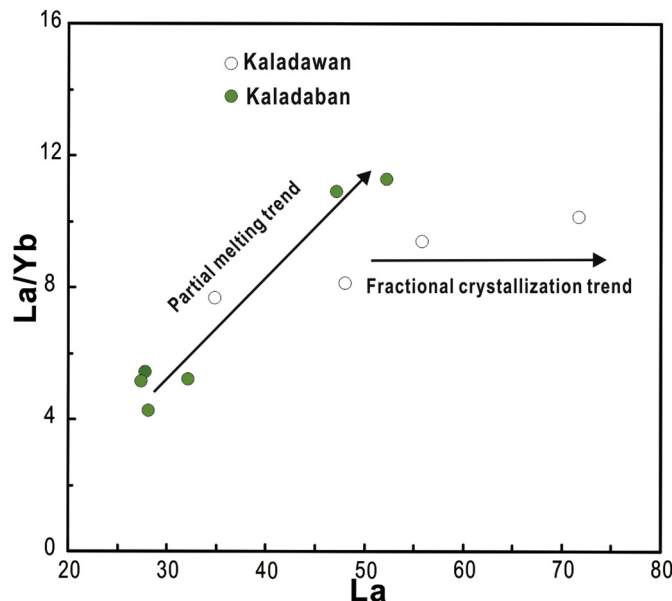


Fig. 14. Plot of La/Yb vs. La for felsic volcanic rocks in the southern Kaladawan district.

$\epsilon_{\text{Hf}}(t)$ value indicates depleted mantle contribution, yet the $^{87}\text{Sr}/^{86}\text{Sr}_i$ values (0.7063–0.7095), $\epsilon_{\text{Nd}}(t)$ values (−9.7 to −1.5), and the two-stages Nd model ages (1.7–1.3 Ga) and $T_{\text{DM2}}(\text{Hf})$ (1.79–1.10 Ga) are all indicative of a crust-dominated mixed source (consisting of an old lower crust and a depleted mantle end-member) (Fig. 10a).

6.3. Early Paleozoic tectonic evolution of the Northern Altyn Mountains

Published geochronological data on the volcanic, ophiolitic and intrusive rocks in the Northern Altyn Mountains are summarized in Table 7. Previous studies proposed a Paleozoic suture in the Northern Altyn based on the presence of ophiolites and HP/UHP metamorphic rocks, which are suggestive of a subduction–collision environment (Che et al., 1995; Sobel and Arnaud, 1999). The NASC ophiolites were likely emplaced during ca. 512–479 Ma (Gao et al., 2011; Yang et al., 2008; L. Zhang et al., 2015a) and represented the remnants of the Proto-Tethys there (Chen et al., 2001). Zhang et al. (2007) reported Cambrian–Ordovician metamorphic ages (ca. 513–491 Ma) for the northern Altyn HP/LT metamorphic rocks, which are similar to or slightly older than the subduction-related magmatisms in the NASC (Chen et al., 2016; Meng et al., 2017). Combined with previous petrological, geochemical and tectonic studies on granitoids from the Northern Altyn Mountains, Wang et al. (2018a, b) proposed that the Kaladawan granites were formed at 476.1 ± 3.3 Ma in an active continental margin (e.g., Liu, 2011; Wu et al., 2007, 2009).

In this study, the high-K calc-alkaline/shoshonite volcanic rocks (basaltic to rhyolitic assemblage) in the southern Kaladawan district are determined to have emplaced at ca. 493–491 Ma, coeval with the regional subductions. In the Ta/Yb vs. Th/Yb diagram (Fig. 15a) and Yb vs. Th/Ta diagram (Fig. 15b), the intermediate volcanic rocks plot in the field of continental arcs while the published mafic volcanic rock samples in north of the Kaladawan area plot in a transitional area between continental arcs and oceanic arcs. A subduction-related petrogenesis for the felsic volcanic rocks is consistent with the volcanic arc affinities shown in the Rb vs. (Nb + Y) and Nb vs. Y tectonic discrimination diagrams (Fig. 15c–d). Thus, these volcanic rocks from the Kaladawan area were interpreted to have formed in a continental island arc. The early Paleozoic MORB-type ophiolites are distributed to the north of the arc magmatic rocks in the northern

Altyn Mountains (Wu et al., 2002; Yang et al., 2008; Yang and Xu, 2002), indicating that the subduction system was likely south-dipping (Fig. 16). Furthermore, the felsic volcanic rocks in the Kaladaban Zn–Pb deposit have higher Rb (Fig. 15c), Y (Fig. 15d), Nb and Th contents than their counterparts in the Kaladawan area. In the Rb vs. (Nb + Y) diagram, the rocks show a geochemical trend from volcanic arc to within-plate affinities, implying that the Kaladaban area was closer to the oceanic side (i.e., Proto-Tethys) and might have formed in a back-arc extension setting.

Summarized the discussions above and previous studies, we proposed a modified tectonic model for the early Paleozoic northern Altyn Mountains (Fig. 16): i) during the late Cambrian–Early Ordovician (510–490 Ma), the Proto-Tethys might have subducted southward beneath the Central Altyn Block. Continuous subductions could have triggered extensive magmatism in the overriding plates and formed the arc intermediate and felsic volcanic rocks in the Kaladawan area (Chen et al., 2016; Cui, 2010; Li et al., 2013). In the back-arc rifting zone, the mafic magma underplatings might have partially melted the lower crusts to form felsic magmas, which were then erupted to form the felsic volcanic rocks and the associated VMS mineralizations at Kaladaban; then, ii) during the Early Ordovician to Silurian (476–440 Ma), the back-arc basin were closed rapidly and formed an active continental margin. Emplacements of granitoids resulted in the developments of skarn Fe–Mo mineralization at Kaladawan.

6.4. Implications for the northern Proto-Tethyan tectonic evolution and metallogeny

The oldest OIB age from the Hongliugou ophiolite, to the west of the Kaladawan district, constrained the minimum age of the Proto-Tethys Ocean opening to 524 Ma (Liu et al., 1999). Based on spatial configurations of arc magmatism, ophiolites, HP/UHP metamorphic rocks and detrital zircon geochronologies, the polarity of the Proto-Tethyan subduction was variably attributed to north-dipping (e.g., Feng et al., 1994; Song et al., 2013; Xia et al., 1996, 2003; Xu et al., 1994; Yang and Xu, 2002), south-dipping (e.g., X. Chen et al., 2009b; Gehrels et al., 2003, 2011; Xiao et al., 2009; Yin et al., 2007) and bipolar (Wu et al., 2010; Zuo and Liu, 1987; Zuo and Wu, 1997). The north-dipping subduction of the Proto-Tethys is not well supported for the lack of arc magmatic rocks in the northern side of the suture. Existence of southward subduction under the CAB is evidenced from the temporal and spatial distributions of arc magmatism and contemporaneous ophiolitic rocks and HP-UHP metamorphic rocks as mentioned above. Timing of the initial subduction of the northern Proto-Tethys Ocean is still poorly constrained. Meng et al. (2017) proposed that the Abei monzogranite (to the north of the Kaladawan, ca. 514 Ma) was formed during the incipient subduction. The monzogranite is closely coeval with the Kaladawan tholeiitic basalt (ca. 517 Ma; Chen et al., 2015), which is also interpreted to have formed during subduction initiation (e.g., Chen et al., 2015; Todd et al., 2012). The subductions had likely generated the Andean-type continental arc intermediate volcanic rocks in the Kaladawan area, whilst the ca. 493–491 Ma felsic volcanic rocks in the Kaladaban VMS deposits were likely erupted in the back-arc spreading center. The closure of the Proto-Tethys in the present Qilian Orogen might have occurred in the earliest Silurian (ca. 443 Ma), as constrained by the youngest arc magmatic rocks there (ca. 443 Ma, Xuanhua Chen et al., 2003a, b), and by the deposition of Silurian volcaniclastic rocks in a probably remnant Proto-Tethyan ocean basin (Yang, 2012).

The concept of mineral systems can be a powerful indicator of tectonic settings and associated evolutionary processes (Bierlein et al., 2009; Chen et al., 2017; Deng et al., 2013, 2016; Groves and Bierlein, 2007; Kesler, 1997). Important hydrothermal mineral deposits related to the subductions of the northern Proto-Tethys

Table 7

Summary of radiometric ages of the volcanic, intrusive, ophiolitic and metamorphic rocks in the Northern Altyn.

Rock type	Sample No.	Sampling location	Dating method	Age	References
Volcanic rocks					
Andesite	KFP-43	Kaladawan	Zircon LA-ICP-MS U–Pb	490.5 ± 5.2 Ma	This study
Rhyolite	KBY2-21	Kaladaban Pb–Zn deposit	Zircon LA-ICP-MS U–Pb	492.6 ± 2.9 Ma	This study
Rhyolite	KBY2-22	Kaladaban Pb–Zn deposit	Zircon LA-ICP-MS U–Pb	491.6 ± 5.6 Ma	This study
Felsic volcanic rock	H378-1	Lapeiquan	Zircon SHRIMP U–Pb	482.7 ± 5.6 Ma	Chen et al., 2016
Andesitic basalt		Baba iron deposit	Zircon SHRIMP U–Pb	517 ± 7 Ma	Chen et al., 2016
Rhyolitic crystal tuff	H365-3	Kaladaban	Zircon SHRIMP U–Pb	485.4 ± 3.9 Ma	Chen et al., 2016
Rhyolitic crystal tuff	H367-5	Kaladaban	Zircon SHRIMP U–Pb	482.0 ± 5.1 Ma	Chen et al., 2016
Andesite	H365-12	Kaladaban	Zircon SHRIMP U–Pb	482.3 ± 4.4 Ma	Chen et al., 2016
Felsic volcanic rock	H360-1	Kaladaban West Cu–Pb–Zn deposit	Zircon SHRIMP U–Pb	477.6 ± 4.9 Ma	Chen et al., 2016
Felsic volcanic rock	H361-1	Kaladaban West Cu–Pb–Zn deposit	Zircon SHRIMP U–Pb	483.7 ± 4.8 Ma	Chen et al., 2016
Basalt	TR-050-13-1	Qiashenkansayi	Zircon LA-ICP-MS U–Pb	457 ± 14 Ma	Liu et al., 2013
Volcanic clastic rock	09A-60	Hongliugou	Zircon LA-ICP-MS U–Pb	457 ± 4 Ma	Wang, 2011
Volcanic clastic rock	09A-61	Hongliugou	Zircon LA-ICP-MS U–Pb	480 Ma	Wang, 2011
Volcanic clastic rock	09A-17-1	Hongliugou	Zircon LA-ICP-MS U–Pb	474 Ma	Wang, 2011
Trachyandensite		Lapeiquan	Zircon SHRIMP U–Pb	494 ± 23 Ma	Xinjiang XBGMR, 2008
Rhyolitic dacite		Kaladaban West Cu–Pb–Zn deposit	Zircon SHRIMP U–Pb	503 ± 14 Ma	Xinjiang XBGMR, 2008
Ophiolitic rocks					
Gabbro		Hongliugou	Zircon LA-ICP-MS U–Pb	513 ± 3 Ma	Zhang et al., 2015b
Plagioclase granite	09HLG07	Hongliugou	Zircon LA-ICP-MS U–Pb	512.1 ± 1.5 Ma	Gao et al., 2011
Gabbro	XVI-2	Binggou	Zircon SHRIMP U–Pb	449.5 ± 10.9 Ma	Yang, 2012
Basalt		Beiketan	Zircon SHRIMP U–Pb	446 ± 10 Ma	Xinjiang XBGMR, 2009a
Gabbro	08K5-VIII-2	Zhuoabulake	Zircon SHRIMP U–Pb	443 ± 12 Ma	Xinjiang XBGMR, 2009b
Gabbro		Hongliugou	Zircon SHRIMP U–Pb	479.4 ± 8.5 Ma	Yang et al., 2008
Pillow basalt	IV-335	Qiashenkansayi	Zircon TIMS U–Pb	448.6 ± 3.3 Ma	Xiu et al., 2007
Mafic lavas (OIB)		Beiketan	Whole-rock Sm–Nd	524.4 Ma	Liu et al., 1999
Pillow basalt (MORB)		Qiashenkansayi	Whole-rock Sm–Nd	508.3 ± 41–512.9 ± 44 Ma	Liu et al., 1999
Intrusive rocks					
Granite	KFP-4	Kaladawan Fe–Mo orefield	Zircon LA-ICP-MS U–Pb	476.1 ± 3.3 Ma	Wang et al., 2018a
Granodiorite	14A-53	Baijianshan	Zircon LA-ICP-MS U–Pb	475.2 ± 2.0 Ma	Liu et al., 2017a
Monzogranite	07A001-3	Abei	Zircon SHRIMP U–Pb	514.3 ± 5.6 Ma	Meng et al., 2017
Granodiorite	10H262-2	4377 Highland	Zircon SHRIMP U–Pb	494.4 ± 5.5 Ma	Meng et al., 2017
Quartz diorite	14K908-3	Kaladawan	Zircon SHRIMP U–Pb	477.0 ± 3.7 Ma	Meng et al., 2017
Monzogranite	12K429-3	Kaladawan	Zircon SHRIMP U–Pb	459.5 ± 6.4 Ma	Meng et al., 2017
Deformed diorite	K272-1	Abei	Zircon LA-ICP-MS U–Pb	478.1 ± 2.1 Ma	Wu et al., 2016
Biotite monzogranite	B-2	Abei	Zircon SHRIMP U–Pb	427.3 ± 5.7 Ma	Meng et al., 2016
Granodiorite	B2	4377 Highland	Zircon SHRIMP U–Pb	494.4 ± 5.5 Ma	Meng et al., 2015
Granite	H01-3	Abei	Zircon SHRIMP U–Pb	514 ± 6 Ma	Han et al., 2012
Granite	H25-1	Abei	Zircon SHRIMP U–Pb	417 ± 5 Ma	Han et al., 2012
Porphyritic monzogranite	H31-1	East of Baijianshan	Zircon SHRIMP U–Pb	431 ± 4 Ma	Han et al., 2012
Granite	H139-1	South of Kaladawan	Zircon SHRIMP U–Pb	479 ± 4 Ma	Han et al., 2012
Granite	H352-2	South of Kaladawan	Zircon SHRIMP U–Pb	488 ± 5 Ma	Han et al., 2012
Quartz diorite	H70-3	South of Kaladawan	Zircon SHRIMP U–Pb	477 ± 4 Ma	Han et al., 2012
Granodiorite	H272-1	4377 Highland	Zircon SHRIMP U–Pb	506.2 ± 2.3 Ma	Han et al., 2012
Granite	H247-1	Dapinggou	Zircon SHRIMP U–Pb	477.1 ± 4.7 Ma	Han et al., 2012
Granodiorite		West of Zhuoabulake	Zircon SHRIMP U–Pb	439.6 ± 3.5 Ma	Han et al., 2012
Granite		South of Bashenkaogong basin	Zircon SHRIMP U–Pb	461.7 ± 12.7 Ma	Yang, 2012
Granite		North of Qiashenkansayi	Zircon SHRIMP U–Pb	419.9 ± 7.9 Ma	Yang, 2012
Granite		Kalashan-Binggou	Zircon TIMS U–Pb	418.5 ± 9.6 Ma	Yang, 2012
Granite		Kalashan-Binggou	Zircon TIMS U–Pb	410.7 ± 11.9 Ma	Yang, 2012
Gabbro		Qilesayi	Zircon LA-ICP-MS U–Pb	477.5 ± 3.3 Ma	Zhang et al., 2012
Diorite		Qilesayi	Zircon LA-ICP-MS U–Pb	469.7 ± 3.4 Ma	Zhang et al., 2012
Granite	09A-59	Hongliugou	Zircon LA-ICP-MS U–Pb	500.3 ± 1.2 Ma	Kang et al., 2011
Porphyritic granite	CL03-107A	South of Bashenkaogong basin	Zircon SHRIMP U–Pb	434.5 ± 3.8 Ma	Wu et al., 2009
porphyritic granite	CL03-121A	South of Bashenkaogong basin	Zircon SHRIMP U–Pb	431.1 ± 3.8 Ma	Wu et al., 2009
Porphyritic granite	CL03-125A	South of Bashenkaogong basin	Zircon SHRIMP U–Pb	474.3 ± 6.8 Ma	Wu et al., 2009
Aphyric granite	CL03-141A	South of Bashenkaogong basin	Zircon SHRIMP U–Pb	446.6 ± 5.2 Ma	Wu et al., 2009
Diorite		Lapeiquan	Zircon TIMS U–Pb	472.3 ± 0.8 Ma	Xinjiang XBGMR, 2008
Quartz diorite	K29-31	North of Bashenkaogong basin	Zircon SHRIMP U–Pb	481.6 ± 5.6 Ma	Wu et al., 2007
Granite	CL03-108A	North of Bashenkaogong basin	Zircon SHRIMP U–Pb	433.1 ± 3.4 Ma	Wu et al., 2007
Granite	CL03-132A	North of Bashenkaogong basin	Zircon SHRIMP U–Pb	437 ± 3 Ma	Wu et al., 2007
Granite	CL03-171A	North of Bashenkaogong basin	Zircon SHRIMP U–Pb	434.6 ± 1.6 Ma	Wu et al., 2007
Granite	K30-1	North of Bashenkaogong basin	Zircon SHRIMP U–Pb	443 ± 11 Ma	Wu et al., 2007
Granodiorite		Jinyanshan	Zircon TIMS U–Pb	467.1 ± 6 Ma	Hao et al., 2006
Granodiorite	HLG-17	North of Qiashenkansayi	Zircon SHRIMP U–Pb	481.5 ± 5.3 Ma	Qi et al., 2005
Granite	HLG-14	North of Qiashenkansayi	Zircon SHRIMP U–Pb	404.7 ± 9.8 Ma	Qi et al., 2005
Porphyritic granite	D52-1	Kalashan-Binggou	Zircon TIMS U–Pb	443 ± 5 Ma	Qi et al., 2005
Granite	DP2_1	Dapinggou	Zircon TIMS U–Pb	485 ± 10 Ma	Yang et al., 2004
Granite	AY6-8-99-1	North of Bashenkaogong basin	Zircon TIMS U–Pb	439.6 ± 6.8 Ma	Cowgill et al., 2003
Granite	GA141	Kaladawan	Zircon TIMS U–Pb	482 ± 11 Ma	Gehrels et al., 2003
Granite	GA159	Lapeiquan	Zircon TIMS U–Pb	479 ± 64 Ma	Gehrels et al., 2003
Granite	GA139	Kaladawan	Zircon TIMS U–Pb	413 ± 5 Ma	Gehrels et al., 2003
Metamorphic rocks					

Table 7 (continued)

Rock type	Sample No.	Sampling location	Dating method	Age	References
Two-mica schist	KBY2-20	Kaladaban Zn–Pb deposit	Muscovite Ar–Ar	Isochron age: 448.2 ± 4.4 Ma; plateau age: 451.0 ± 4.1 Ma	Wang et al., 2018b
Eclogite	Q03-3-5.3	Hongliugou	Phengite Ar–Ar	Isochron age: 513 ± 5 Ma; plateau age: 512 ± 3 Ma	Zhang et al., 2007
Blueschist	Q03-1-4.1	Hongliugou	Paragonite Ar–Ar	Isochron age: 497 ± 10 Ma; Plateau age: 491 ± 3 Ma	Zhang et al., 2007
Sericite–quartz schist		Bashenkaogong	Sercicite Ar–Ar	Isochron age: 450 ± 11 Ma; Plateau age: 455 ± 2 Ma	Hao et al., 2006
HP metamorphic rock		East of Beiketan	Phengite Ar–Ar	Isochron age: 572.58 ± 5.52 Ma; High-temperaure plateau age: 574.68 ± 2.50 Ma; Low-temperaure plateau age: 527.39 ± 5.34 Ma, 479.81 ± 4.89 Ma	Liu et al., 1999

mainly include VMS Cu–Zn–Pb deposits, porphyry–skarn Cu, Fe–Mo and Au deposits and epithermal Ag–Au polymetallic deposits. Among these deposit types, VMS is the most common, e.g., northern Qinling: the Tongyu Cu deposit (zircon U–Pb age: 472 ± 11 Ma, Lee et al., 2010); Northern Qilian: the Xiaozhilong Cu deposit (zircon U–Pb age: 458 ± 1 Ma; Cong, 2017); northern Altyn: the Kaladaban Zn–Pb deposit (492.6 ± 2.9 Ma; Wang et al., 2018b). Similar to the Kaladaban orefield, the VMS deposits above-mentioned contain stratiform massive sulfides and lensoidal ore-bodies hosted in early Paleozoic volcanic rocks. Porphyry–skarn deposits include the Langlike Cu deposit in northern Qilian (zircon U–Pb age: 471 ± 3 Ma; Guo et al., 2015), and the Kaladawan Fe–Mo orefield in northern Altyn (zircon U–Pb age: 476.1 ± 3.3 Ma; Wang et al., 2017). The epithermal Ag–Au polymetallic deposits (e.g., the Abei Ag–Pb deposit in north Altyn, zircon U–Pb age: 514 ± 6 Ma) are less economically important and also commonly

considered to be formed by the intrusion-derived hydrothermal fluids (Chen et al., 2012). Skarn and epithermal Au–Ag deposits are mainly formed in magmatic arcs (Einaudi et al., 1981; Meinert et al., 2005), while preserved VMS deposits are formed during arc-related rifting, mostly in backarc basins (Franklin et al., 2005; Hannington et al., 2005). Consequently, the spatial distribution of these deposits in the northern Altyn, i.e., Skarn and epithermal Au–Ag mineral systems are distributed to the north of the VMS systems, also indicates the south-dipping subductions of the Proto-Tethys Ocean.

7. Conclusions

(1) Volcanic rocks in the southern Kaladawan district were erupted at about 492.6–490.5 Ma, probably formed in a south-dipping continental island arc and accompanied by

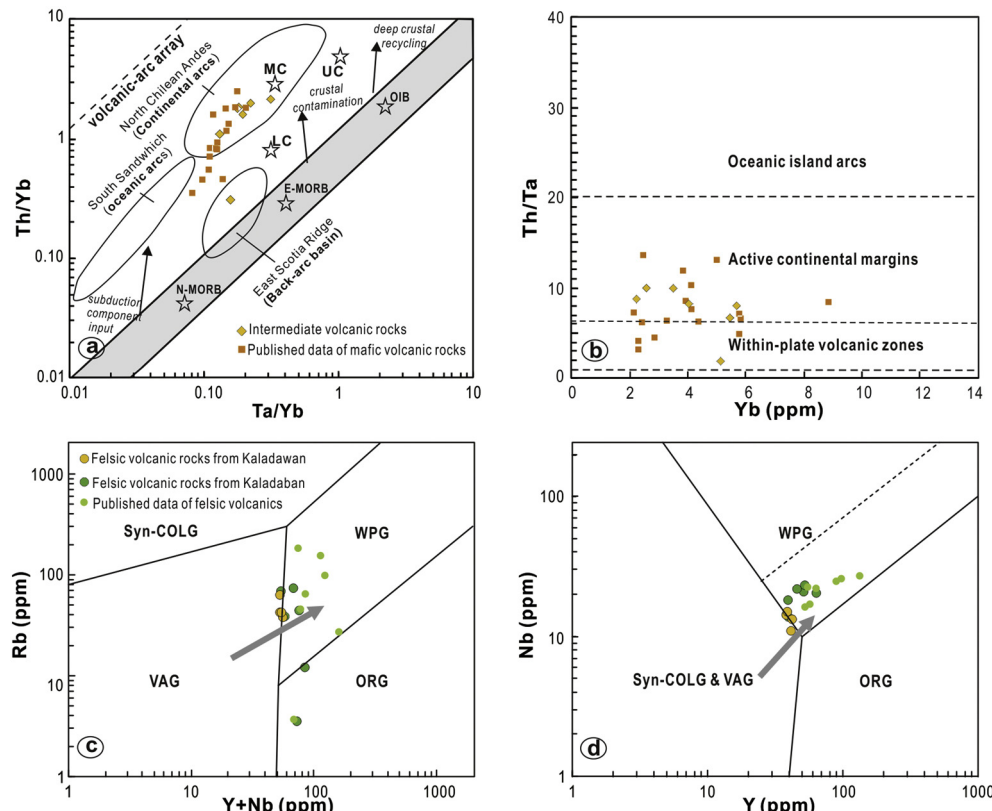


Fig. 15. Tectonic discrimination diagrams for the volcanic rocks in the southern Kaladawan district. (a) Th/Yb vs. Ta/Yb diagram (Pearce and Peate, 1995), also discriminating rocks enriched by subduction, crustal contamination and deep crustal recycling (modified after Pearce, 2008). (b) Th/Ta vs. Yb diagram (after Gorton and Shandl, 2000). Felsic volcanic rocks: (c) Rb vs. Nb + Y diagram (after Pearce et al., 1984). (d) Nb vs. Y diagram (after Pearce et al., 1984). Data for the South Sandwich Island IAB and North Chilean Andes basalt and andesite are from Pearce et al. (1995), for the East Scotia Ridge E-BABB are from Leat et al. (2000) and for volcanic rocks in the northern Altyn are from Cui (2010) and Li et al. (2013). Abbreviations: VAG, volcanic arc granites; ORG, ocean ridge granites; WPG, within-plate granites; Syn-COLG, syn-collision granites; POG, post-collision granites.

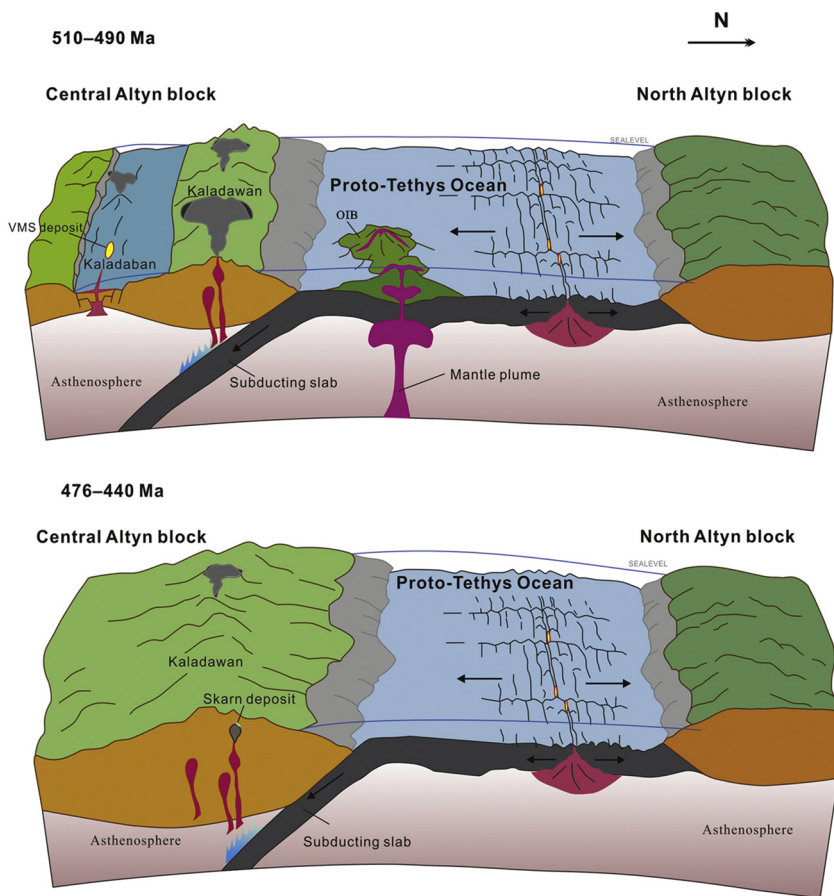


Fig. 16. Schematic tectonic model for the early Paleozoic northern Altyn.

the development of many important VMS, porphyry skarn deposits.

- (2) The intermediate volcanics may have formed by partial melting of the mantle wedge, in response to the introduction of fluids released from the subducted slab with subducted sediment input.
- (3) The Kaladaban felsic volcanic rocks were likely formed by partial melting of the lower crust with contribution of the depleted mantle.

Acknowledgement

This study was funded by the NSFC (41802079, 41672086, 41872085) and China Geological Survey (1212011140056). The authors thank the staffs of the Xinjiang BGMR (esp. Wan-Xiu Qi and Xi-Liang Li) for the field assistance. We are grateful to Yan-Jing Chen, Li Zhang, Deng-Feng Li and Jing Fang for taking part in field survey and to Yue-Jun Wang, Yu-Zhi Zhang, Liang Qi, Chun-Rong Diwu, Le Zhang, Pin Wang, Yan-Shuang Wu, Wei-Feng Zhang and Lian-Dang Zhao for the laboratory assistance and manuscript preparation. Dr. Chun-Kit Lai polished the English of the manuscript. Constructive suggestions, pertinent comments and careful corrections by two anonymous reviewers and Prof. Franco Pirajno greatly improved the quality of the manuscript.

References

- Bierlein, F.P., Groves, D.I., Cawood, P.A., 2009. Metallogeny of accretionary orogens — the connection between lithospheric processes and metal endowment. *Ore Geology Reviews* 36, 282–292. <https://doi.org/10.1016/j.oregeorev.2009.04.002>.
- Blichert-Toft, J., Albarède, F., 1997. The Lu-Hf isotope geochemistry of chondrites and the evolution of the mantle-crust system. *Earth and Planetary Science Letters* 148, 243–258. [https://doi.org/10.1016/S0012-821X\(97\)00040-X](https://doi.org/10.1016/S0012-821X(97)00040-X).
- Cao, H., Li, S., Zhao, S., Yu, S., Li, X., Somerville, I.D., 2016. Detrital zircon geochronology of Neoproterozoic to early Paleozoic sedimentary rocks in the North Qinling Orogenic Belt: Implications for the tectonic evolution of the Kuaping Ocean. *Precambrian Research* 279, 1–16. <https://doi.org/10.1016/j.precamres.2016.04.001>.
- Chauvel, C., Lewin, E., Carpentier, M., Arndt, N.T., Marini, J.-C., 2008. Role of recycled oceanic basalts and sediment in generating the Hf–Nd mantle array. *Nature Geoscience* 1, 64–67. <https://doi.org/10.1038/ngeo.2007.51>.
- Che, Z.C., Liu, L., Liu, H.F., Luo, J.H., 1995. The discovery and occurrence of high-pressure metamorphic rocks from Altyn Mountain area, Xinjiang Autonomous Region. *Chinese Science Bulletin* 40, 1298–1300.
- Chen, Z.L., 1994. Tethyan geology for 100 years. *Tethyan Geol.* 18, 1–22.
- Chen, X., Wang, X., Yang, F., Chen, Z., Chen, B., Wang, K., 2001. Tectonic environments of magmatism in Early Paleozoic in the North Altyn Tagh, China. *J. Geomech.* 7, 193–200.
- Chen, X., Gehrels, G., Wang, X., Yang, F., Chen, Z., 2003. Granite from North Altyn Tagh, NW China: U–Pb geochronology and tectonic setting. *Bulletin of Mineralogy, Petrology and Geochemistry* 22, 294–298.
- Chen, X., Yin, A., Gehrels, G.E., Cowgill, E.S., Grove, M., Harrison, T.M., Wang, X.-F., 2003. Two phases of Mesozoic north-south extension in the eastern Altyn Tagh range, northern Tibetan Plateau. *Tectonics* 22. <https://doi.org/10.1029/2001TC001336> (8–1–8–22).
- Chen, B., Jiang, R., Li, L., Chen, Z., Qi, W., Liu, R., Cui, L., Wang, S., 2009. Discovery of iron ore zones in the Kaladawan Area within the eastern part of the Altun Mountains and its significance. *Acta Geoscientia Sinica* 30, 143–154.
- Chen, X., Yin, A., Gehrels, G.E., Jiang, R., Chen, Z., Bai, Y., 2009. Geothermochronology and tectonic evolution of Eastern Altyn Tagh Mountains, Northwestern China. *Earth Science Frontiers* 16, 207–219.
- Chen, B., Cao, F., Zhao, S., Li, C., Zhao, H., Li, J., Chen, Z., Ren, Y., Li, Y., Liu, W., Li, J., Huang, J., Yang, Y., Cui, L., 2011. Fold structure and its origin in the Dapinggou area, eastern Altun Mountains. *Geological Bulletin of China* 30, 1934–1940.
- Chen, B.L., Zhao, H., Le, Ma, Y.Z., Yang, F., Wang, S.X., Chen, Z., Le, Qi, W., Liu, R., Jiang, R.B., Li, L., 2012. A preliminary discussion on genesis and structural control of Abei silver-lead deposit in eastern Altun Mountains. *Mineralium Deposita* 31, 13–26.
- Chen, B., Yong, W., Chen, Z., Songbin, L.I., Jiang, R., Han, F., Cui, L., Li, L.I., Zhao, S., Wanxiu, Q.I., 2015. A study of the structural system of ore-forming and ore-controlling in Kaladawan ore clustering area, Altun Tagh Mountains, NW China. *Earth Science Frontiers* 22, 67–77.
- Chen, B., Li, S., Jiang, R., Chen, Z., Han, F., Cui, L., Li, L., Zhao, S., Qi, W., Yang, Y.,

- Wang, S., Wang, Y., Zhou, Y., Hao, R., 2016. Zircon SHRIMP U-Pb dating of intermediate-felsic volcanic rocks from the Kaladawan Area, Altun Mountains and its tectonic environment. *Acta Geologica Sinica* 90, 708–727.
- Chen, Y.J., Zhang, C., Wang, P., Pirajno, F., Li, N., 2017. The Mo deposits of Northeast China: a powerful indicator of tectonic settings and associated evolutionary trends. *Ore Geology Reviews* 81, 602–640. <https://doi.org/10.1016/j.oregeorev.2016.04.017>.
- Chernyshev, I.V., Chugaev, A.V., Shatagin, K.N., 2007. High-precision Pb isotope analysis by multicollector-ICP-mass-spectrometry using 205TI/203TI normalization: Optimization and calibration of the method for the studies of Pb isotope variations. *Geochemistry International* 45, 1065–1076. <https://doi.org/10.1134/S0016702907110018>.
- Class, C., Miller, D.M., Goldstein, S.L., Langmuir, C.H., 2000. Distinguishing melt and fluid subduction components in Umnak Volcanics, Aleutian Arc. *Geochemistry, Geophysics, Geosystems* 1, 1. <https://doi.org/10.1029/1999GC000010>.
- Cong, Z., 2017. Study on Metallogenetic Regularity of Copper Polymetallic Deposit in the North Qilian, Qinghai. Jinlin University.
- Cowgill, E., Yin, A., Harrison, T.M., Xiao-Feng, W., 2003. Reconstruction of the Altyn Tagh fault based on U-Pb geochronology: Role of back thrusts, mantle sutures, and heterogeneous crustal strength in forming the Tibetan Plateau. *Journal of Geophysical Research - Solid Earth* 108, 2346. <https://doi.org/10.1029/2002JB002080>.
- Cui, L.L., 2010. The Characteristics and Genetic Analysis of Kaladaban Pb-Zn Deposit, East of Altyn Tagh (Thesis). Chinese Academy of Geological Sciences.
- Deng, X.H., Chen, Y.J., Santosh, M., Yao, J.M., 2013. Genesis of the 1.76Ga Zhaiwa Mo-Cu and its link with the Xionger volcanics in the North China Craton: Implications for accretionary growth along the margin of the Columbia supercontinent. *Precambrian Research* 227, 337–348. <https://doi.org/10.1016/j.precamres.2012.02.014>.
- Deng, X.H., Chen, Y.J., Santosh, M., Yao, J.M., Sun, Y.L., 2016. Re-Os and Sr-Nd-Pb isotope constraints on source of fluids in the Zhifang Mo deposit, Qinling Orogen, China. *Gondwana Research* 30, 132–143. <https://doi.org/10.1016/j.gr.2015.06.020>.
- Dong, Y., Zhang, G., Hauzenberger, C., Neubauer, F., Yang, Z., Liu, X., 2011. Palaeozoic tectonics and evolutionary history of the Qinling orogen: evidence from geochemistry and geochronology of ophiolite and related volcanic rocks. *Lithos* 122, 39–56. <https://doi.org/10.1016/j.lithos.2010.11.011>.
- Dong, Y., Zhang, G., Neubauer, F., Liu, X., Genser, J., Hauzenberger, C., 2011. Tectonic evolution of the Qinling orogen, China: Review and synthesis. *Journal of Asian Earth Sciences* 41, 213–237. <https://doi.org/10.1016/j.jseas.2011.03.002>.
- Einaudi, M.T., Meinert, L.D., Newberry, R.J., 1981. Skarn deposits. *Economic Geology* 31–391 (75th Anniv.).
- Farmer, G.L., DePaolo, D.J., 1987. Nd and Sr isotope study of hydrothermally altered granite at San Manuel, Arizona; implications for element migration paths during the formation of porphyry copper ore deposits. *Economic Geology* 82, 1142–1151. <https://doi.org/10.2113/gsecongeo.82.5.1142>.
- Faure, G., 1977. Principles of Isotope Geology. Smith and Wyllie Intermediate Geology Series. Smith and Wyllie Intermediate Geology Series.
- Feng, Y., He, S., Yan, J., 1994. The discovery and geological significance of sheeted dyke complex in the Early-Middle Ordovician ophiolite in the central section of the North Qilian Mountains, China. *Ore Geology Reviews* 40, 252–265.
- Franklin, J.M., Gibson, H.L., Jonasson, I.R., Galley, A.G., 2005. Volcanogenic massive sulfide deposits. *Economic Geology* 111, 523–560. [https://doi.org/10.1016/0169-1368\(95\)00022-4](https://doi.org/10.1016/0169-1368(95)00022-4) (100th Anniv.).
- Gao, X.F., Xiao, P.X., Guo, L., Dong, Z.C., Xi, R.G., 2011. Opening of an early Paleozoic limited oceanic basin in the northern Altyn area: Constraints from plagiogranites in the Hongliugou-Lapeiquan ophiolitic mélange. *Science in China Series D: Earth Sciences* 54, 1871–1879. <https://doi.org/10.1007/s11430-011-4332-9>.
- Ge, X.H., Liu, J., 1999. Formation and tectonic background of the Northern Qilian Orogenic Belt. *Earth Science Frontiers* 6, 223–230.
- Gehrels, G.E., Yin, A., Wang, X.-F., 2003. Magmatic history of the northeastern Tibetan Plateau. *Journal of Geophysical Research - Solid Earth* 108, 1–14. <https://doi.org/10.1029/2002JB001876>.
- Gehrels, G., Kapp, P., DeCelles, P., Pullen, A., Blakey, R., Weislogel, A., Ding, L., Guynn, J., Martin, A., McQuarrie, N., Yin, A., 2011. Detrital zircon geochronology of pre-Tertiary strata in the Tibetan-Himalayan orogen. *Tectonics* 30. <https://doi.org/10.1029/2011TC002868>.
- Gorton, M.P., Shandl, E.S., 2000. From continents to island arcs: a geochemical index of tectonic setting for arc-related and within-plate felsic to intermediate volcanic rocks. *The Canadian Mineralogist* 38, 1065–1073. <https://doi.org/10.2113/gscanmin.38.5.1065>.
- Griffin, W.L., Pearson, N.J., Belousova, E., Jackson, S.E., van Achterbergh, E., O'Reilly, S.Y., Shee, S.R., 2000. The Hf isotope composition of cratonic mantle: LAM-MC-ICPMs analysis of zircon megacrysts in kimberlites. *Geochimica et Cosmochimica Acta* 64, 133–147. [https://doi.org/10.1016/S0016-7037\(99\)00343-9](https://doi.org/10.1016/S0016-7037(99)00343-9).
- Griffin, W.L., Wang, X., Jackson, S.E., Pearson, N.J., O'Reilly, S.Y., Xu, X., Zhou, X., 2002. Zircon chemistry and magma mixing, SE China: In-situ analysis of Hf isotopes, Tonglu and Pingtan igneous complexes. *Lithos* 61, 237–269. [https://doi.org/10.1016/S0024-4937\(02\)00082-8](https://doi.org/10.1016/S0024-4937(02)00082-8).
- Groves, D.I., Bierlein, F.P., 2007. Geodynamic settings of mineral deposit systems. *Journal of the Geological Society of London* 164, 19–30. <https://doi.org/10.1144/0016-76492006-065>.
- Guo, F.X., 2001. Paleoozoic tectono-paleobiogeography of Xinjiang, China. *Xinjiang Geology* 19, 20–26.
- Guo, Z., Bai, Y., Zhao, X., Kong, H., Tan, W., Jiang, H., Li, C., Zhang, H., 2015. Geochronology and Geochemistry of Magnesian Andesites in the Langlike Copper Deposit, North Qilian Shan, China. *Geology and Exploration* 51, 253–265.
- Han, F., Bin, Chen, B.L., Cui, L.L., Wang, S.X., Chen, Z., Le, Jiang, R.B., Li, L., Qi, W.X., 2012. Zircon SHRIMP U-Pb age of intermediate-acid intrusive rocks in Kaladawan area, eastern Altun Mountains, NW China, and its implications. *Acta Petrologica Sinica* 28, 2277–2291.
- Hannington, M.D., de Ronde, C.E.J., Petersen, S., 2005. Sea-floor tectonics and submarine hydrothermal systems. *Econ. Geol.* 100th Anniv. 111–141.
- Hao, J., Wang, E.Q., Liu, X.H., Sang, H.Q., 2006. Jinyanshan collisional orogenic belt of the early Paleozoic in the Altun mountains:evidence from single zircon U-Pb and 40 Ar/39 Ar isotopic dating for the arc magmatic and ophiolitic mélange. *Acta Petrologica Sinica* 22, 2743–2752.
- Hao, R., Chen, B., Chen, Z., Wang, Y., Li, S., Han, F., Zhou, Y., 2013. Geochemical characteristics of Basalts from Kaladawan in East Altun Mountains of Xinjiang and their implications. *Acta Geoscientia Sinica* 34, 307–317.
- Harmon, R.S., Thorpe, R.S., Francis, P.W., 1981. Petrogenesis of Andean andesites from combined O-Sr isotope relationships. *Nature* 290, 396–399.
- Hastie, A.R., Kerr, A.C., Pearce, J.A., Mitchell, S.F., 2007. Classification of altered volcanic island arc rocks using immobile trace elements: development of the Th-Co discrimination diagram. *Journal of Petrology* 48, 2341–2357. <https://doi.org/10.1093/petrology/egm062>.
- Hawkesworth, C.J., Gallagher, K., Hergt, J.M., McDermott, F., 1993. Mantle and slab contributions in arc magmas. *Annual Review of Earth and Planetary Sciences* 21, 175–204. <https://doi.org/10.1017/CBO9781107415324.004>.
- He, G.Q., Cheng, S.D., Xu, X., Li, J.Y., Hao, J., 2004. Tectonic Map of Xinjiang Uygur Autonomous Region and its Adjacent Areas.
- Hofmann, A.W., 1988. Chemical differentiation of the Earth: the relationship between mantle, continental crust, and oceanic crust. *Earth and Planetary Science Letters* 90, 297–314. [https://doi.org/10.1016/0012-821X\(88\)90132-X](https://doi.org/10.1016/0012-821X(88)90132-X).
- Jacobsen, S.B., Wasserburg, G.J., 1980. Sm-Nd isotopic evolution of chondrites. *Earth and Planetary Science Letters* 50, 139–155. [https://doi.org/10.1016/0012-821X\(80\)90125-9](https://doi.org/10.1016/0012-821X(80)90125-9).
- Kang, L., Liu, L., Cao, Y.T., Wang, C., Yang, W.Q., Zhu, X.F., 2011. Geochemistry, zircon LA-ICP-MS U-Pb ages and Hf isotopes of Hongliugou moyite from north Altyn Tagh tectonic belt. *Geological Bulletin of China* 30, 1066–1076.
- Kesler, S.E., 1997. Metallogenetic evolution of convergent margins: selected ore deposit models. *Ore Geology Reviews* 12, 153–171. [https://doi.org/10.1016/S0169-1368\(97\)00007-3](https://doi.org/10.1016/S0169-1368(97)00007-3).
- Kessel, R., Schmidt, M.W., Ulmer, P., Pettke, T., 2005. Trace element signature of subduction-zone fluids, melts and supercritical liquids at 120–180 km depth. *Nature* 437, 724–727. <https://doi.org/10.1038/nature03971>.
- Leat, P.T., Livermore, R.A., Millar, I.L., Pearce, J.A., 2000. Magma supply in back-arc spreading Centre segment E2, East Scotia Ridge. *Journal of Petrology* 41, 845–866. <https://doi.org/10.1093/petrology/41.6.845>.
- Lee, B., Zhu, L.M., Zhang, G.W., Guo, B., Gong, H.J., Yao, A.P., 2010. Geological characteristics, metallogenetic background, and genesis of the Tongyu VHMS copper deposit in the west part of the North Qinling, Shaanxi Province. *Science China Earth Sciences* 53, 1460–1485. <https://doi.org/10.1007/s11430-010-4054-4>.
- Li, X.Z., Yin, F.Y., 2002. Comparation study of the geological structure of the East and West Kunlun Mountains. *Geological Bulletin of China* 21, 777–783.
- Li, X.Z., Pan, G., Luo, J.N., 1990. A boundary between Gonwanaland and Laurasia continents in Sanjiang region. In: *Geological Memoirs of Qinghai-Xizang Plateau*, vol. 20. *Geological Tectonics of "Sanjiang."* Geological Publishing House, Beijing, pp. 217–233.
- Li, X.Z., Liu, Z.G., Pan, G.T., 1991. Geological evolution and division of tectonic units of the Sanjiang Area of Southwest China. *Bull. Chinese Acad. Geol. Sci.* 13.
- Li, X.-H., Long, W.-G., Li, Q.-L., Liu, Y., Zheng, Y.-F., Yang, Y.-H., Chamberlain, K.R., Wan, D.-F., Guo, C.-H., Wang, X.-C., Tao, H., 2010. Penglai zircon megacrysts: a potential New working reference material for microbeam determination of Hf-O isotopes and U-Pb age. *Geostandards and Geoanalytical Research* 34, 117–134. <https://doi.org/10.1111/j.1751-908X.2010.00036.x>.
- Li, W.C., Pan, G.T., Hou, Z.Q., Mo, X.X., Wang, L.Q., Ding, J., Xu, Q., 2010. Archipelagic-Basin, Forming Collision Theory and Prospecting Techniques along the Niujiang-Lancangjiang-Jinshajiang Area in Southwestn China. *Geologic Publishing House, Beijing*.
- Li, S., Chen, B., Chen, Z., Hao, R., Zhou, Y., Han, F., 2013. Geochemistry and Tectonic Implications of the Early Paleozoic Felsic to Intermediate Volcanic Rocks from Kaladawan Area, North Altyn. *Ore Geology Reviews* 59, 423–436.
- Liu, J.H., Liu, L., Gai, Y.S., Kang, L., Yang, W.Q., Liao, X.Y., Yang, M., 2017. Zircon U-Pb dating and Hf isotopic compositions of the Baijianshan granodiorite in North Altyn Tagh and its geological significance. *Acta Geol. Sin.* 1022–1038.
- Li, S., Zhao, S., Liu, X., Cao, H., Yu, S., Li, X., Somerville, I., Yu, S., Suo, Y., 2017. Closure of the Proto-Tethys Ocean and Early Paleozoic amalgamation of micro-continental blocks in East Asia. *Earth-Science Reviews*. <https://doi.org/10.1016/j.earscirev.2017.01.011>.
- Liu, H., 2011. Breakup and closure evolution progress of the North Altyn Ocean from Neoproterozoic to Early Paleozoic—Analyses on the Hongliugou-Lapeiquan ophiolite tectonic mixtite belt (Master Thesis). China University of Geosciences, Wuhan (84pp.).
- Liu, L., Che, Z., Wang, Y., Luo, J., Chen, D., 1999. The petrological characters and geotectonic setting of high-pressure metamorphic rock belts in Altun mountains. *Acta Petrologica Sinica* 15, 57–64.
- Liu, Y., Hu, Z., Gao, S., Günther, D., Xu, J., Gao, C., Chen, H., 2008. In situ analysis of major and trace elements of anhydrous minerals by LA-ICP-MS without applying an internal standard. *Chemical Geology* 257, 34–43. <https://doi.org/10.1016/j.chemgeo.2008.02.001>.

- 1016/j.chemgeo.2008.08.004.
- Liu, Y.S., Yu, H.F., Xin, H.T., Lu, S.N., Xiu, Q.Y., Li, Q., 2009. Tectonic units division and Precambrian significant geological events in Altyn Tagh Mountain, China. *Geological Bulletin of China* 28, 1430–1438.
- Liu, H., Wang, G.C., Yang, Z.J., Luo, Y.J., Gao, R., 2013. Geochronology and geochemistry of the Qashikansayi basalt and its constraint on the closure progress of the North Altyn Ocean. *Acta Geologica Sinica* 87, 38–54.
- Liu, L., Liao, X., Wang, Y., Wang, C., Santosh, M., Yang, M., Zhang, C., Chen, D., 2016. Early Paleozoic tectonic evolution of the North Qinling Orogenic Belt in Central China: Insights on continental deep subduction and multiphase exhumation. *Earth-Science Reviews* 159, 58–81. <https://doi.org/10.1016/j.earscirev.2016.05.005>.
- Lu, S.N., 2001. From Rodinia to Gondwanaland supercontinents: thinking about problems of researching Neoproterozoic supercontinents. *Earth Sci. Front.* 8, 441–448.
- Meinert, L.D., Dipple, G.M., Nicolescu, S., 2005. World skarn deposits. *Economic Geology* 299–336 (100th Anniv.).
- Meng, L., Chen, B., Luo, D., Wang, Y., Sun, Y., Wu, Y., Zhang, H., Wang, T., 2015. SHRIMP Zircon U-Pb Geochronology of northern Highland 4337 granodiorite in Kaladawan area of northern Altun Mountains and its tectonic implications. *Journal of Jilin University (Earth Science Edition)* 45, 1757–1771. <https://doi.org/10.13278/j.cnki.jjuese.201506116>.
- Meng, L.T., Chen, B.L., Wang, Y., Sun, Y., Wu, Y., Zhang, W.G., He, J.T., 2016. Timing of early Paleozoic tectonic regime transition in north Altun: evidence from granite. *Geotectonika et Metallogenika* 40, 295–307.
- Meng, L.T., Chen, B.L., Zhao, N.N., Wu, Y., Zhang, W.G., He, J.T., Wang, B., Han, M.M., 2017. The distribution, geochronology and geochemistry of early Paleozoic granitoid plutons in the North Altun orogenic belt, NW China: implications for the petrogenesis and tectonic evolution. *Lithos* 268–271, 399–417. <https://doi.org/10.1016/j.lithos.2016.10.022>.
- Mo, X., Hou, Z., Niu, Y., Dong, G., Qu, X., Zhao, Z., Yang, Z., 2007. Mantle contributions to crustal thickening during continental collision: evidence from Cenozoic igneous rocks in southern Tibet. *Lithos* 96, 225–242. <https://doi.org/10.1016/j.lithos.2006.10.005>.
- Nowell, G.M., Kempton, P.D., Noble, S.R., Fitton, J.G., Saunders, A.D., Mahoney, J.J., Taylor, R.N., 1998. High precision Hf isotope measurements of MORB and OIB by thermal ionisation mass spectrometry: insights into the depleted mantle. *Chemical Geology* 149, 211–233. [https://doi.org/10.1016/S0009-2541\(98\)00036-9](https://doi.org/10.1016/S0009-2541(98)00036-9).
- Pearce, J.A., 1996. A user's guide to basalts discrimination diagrams. Trace element geochemistry of volcanic rocks: applications for massive sulphide exploration. *Geol. Assoc. Canada, Short Course Notes* 12, 113.
- Pearce, J.A., 2008. Geochemical fingerprinting of oceanic basalts with applications to ophiolite classification and the search for Archean oceanic crust. *Lithos* 100, 14–48. <https://doi.org/10.1016/j.lithos.2007.06.016>.
- Pearce, J.A., Peate, D.W., 1995. Tectonic implications of the composition of volcanic arc magmas. *Annual Review of Earth and Planetary Sciences* 23, 251–285. <https://doi.org/10.1146/annurev.ea.23.050195.001343>.
- Pearce, J.A., Harris, N.B.W., Tindle, A.G., 1984. Trace element discrimination diagrams for the tectonic interpretation of granitic rocks. *Journal of Petrology* 25, 956–983. <https://doi.org/10.1093/petrology/25.4.956>.
- Pearce, J.A., Baker, P.E., Harvey, P.K., Luff, I.W., 1995. Geochemical evidence for subduction fluxes, mantle melting and fractional crystallization beneath the South Sandwich Island Arc. *Journal of Petrology* 36, 1073–1109. <https://doi.org/10.1093/petrology/36.4.1073>.
- Peucat, J.J., Vidal, P., Bernard-Griffiths, J., Condie, K.C., 1989. Sr, Nd, and Pb isotopic systematics in the Archean low- to high-grade transition zone of Southern India: syn-accretion vs. post-accretion granulites. *Journal of Geology* 97, 537–549. <https://doi.org/10.1086/629333>.
- Plank, T., Langmuir, C.H., 1993. Tracing trace elements from sediment input to volcanic output at subduction zones. *Nature* 362, 739–743. <https://doi.org/10.1038/362739a0>.
- Plank, T., Langmuir, C.H., 1998. The chemical composition of subducting sediment and its consequences for the crust and mantle. *Chemical Geology* 145, 325–394. [https://doi.org/10.1016/S0009-2541\(97\)00150-2](https://doi.org/10.1016/S0009-2541(97)00150-2).
- Platzner, I., Ehrlich, S., Halicz, L., 2001. Isotope-ratio measurements of lead in NIST standard reference materials by multiple-collector inductively coupled plasma mass spectrometry. *Fresenius' Journal of Analytical Chemistry* 370, 624–628. <https://doi.org/10.1007/s002160100875>.
- Polet, A., Münker, C., 2004. Hf-Nd isotope evidence for contemporaneous subduction processes in the source of late Archean arc lavas from the Superior Province, Canada. *Chemical Geology* 213, 403–429. <https://doi.org/10.1016/j.chemgeo.2004.08.016>.
- Qi, L., Hu, J., Conrad, D., Gregoire, D.C., 2000. Determination of trace elements in granites by inductively coupled plasma mass spectrometry. *Talanta* 51, 507–513. [https://doi.org/10.1016/S0039-9140\(99\)00318-5](https://doi.org/10.1016/S0039-9140(99)00318-5).
- Qi, X.X., Li, H.B., Wu, C.L., Yang, J.S., Zhang, J.X., Meng, F.C., Shi, D.R., Chen, S.Y., 2005. Zircon SHRIMP U-Pb dating of the Qashikansayi granodiorite from North Altyn and its geological significances. *Scientific Bulletin* 50, 571–576.
- von Raumer, J.F., Stampfli, G.M., 2008. The birth of the Rheic Ocean — Early Palaeozoic subsidence patterns and subsequent tectonic plate scenarios. *Tectonophysics* 461, 9–20. <https://doi.org/10.1016/j.tecto.2008.04.012>.
- Raymond, L.A., 1995. Petrology: the study of igneous, sedimentary, metamorphic rocks. Dubuque, Iowa: Wm. C. Brown.
- Rudnick, R.L., Gao, S., 2003. 3.01—composition of the continental crust. In: Holland, H.D., Turekian, K.K. (Eds.), *Treatise on Geochemistry*. Elsevier-
- Pergaman, Oxford, pp. 1–64. <https://doi.org/10.1016/B0-08-043751-6/03016-4>.
- Salters, V.J.M., Stracke, A., 2004. Composition of the depleted mantle. *Geochemistry, Geophysics, Geosystems* 5. <https://doi.org/10.1029/2003GC000597>.
- Scherer, E., Munker, C., Mezger, K., 2001. Calibration of the lutetium-hafnium clock. *Science* (80-). 293, 683–687. doi:DOI <https://doi.org/10.1126/science.1061372>.
- Şengör, A.M.C., Natal'in, B.A., 1996. Paleotectonics of Asia: fragments of synthesis. In: Yin, A., Harrison, T.M. (Eds.), *The Tectonic Evolution of Asia*. Cambridge University Press, Cambridge, pp. 486–640.
- Shinjo, R., Kato, Y., 2000. Geochemical constraints on the origin of bimodal magmatism at the Okinawa Trough, an incipient back-arc basin. *Lithos* 54, 117–137. [https://doi.org/10.1016/S0024-4937\(00\)00034-7](https://doi.org/10.1016/S0024-4937(00)00034-7).
- Sobel, E.R., Arnaud, N., 1999. A possible middle Paleozoic suture in the Altyn Tagh, NW China. *Tectonics* 18, 64–74. <https://doi.org/10.1029/1998TC900023>.
- Song, S., Niu, Y., Su, L., Xia, X., 2013. Tectonics of the North Qilian orogen, NW China. *Gondwana Research* 23, 1378–1401. <https://doi.org/10.1016/j.gr.2012.02.004>.
- Steiger, R.H., Jäger, E., 1977. Subcommission on geochronology: convention on the use of decay constants in geo- and cosmochronology. *Earth and Planetary Science Letters* 36, 359–362. [https://doi.org/10.1016/0012-821X\(77\)90060-7](https://doi.org/10.1016/0012-821X(77)90060-7).
- Sun, S.S., McDonough, W.F., 1989. Chemical and isotopic systematics of oceanic basalts: implications for mantle composition and processes. *Geol. Soc. Spec. Publ.* 42, 313–345. <https://doi.org/10.1144/GSL.SP.1989.042.01.19>.
- Sun, Y., Liu, C.Y., Chi, Z.C., 1997. The Proterozoic rift volcanic series in the Lapeiquan area, the Altyn Mountains and its tectonic significance. *Geol. Rev.* 43, 17–24.
- Thorpe, R.S., Francis, P.W., Moorbat, S., 1979. Strontium isotope evidence for petrogenesis of Central American andesites. *Nature* 277, 44–45.
- Todd, E., Gill, J.B., Pearce, J.A., 2012. A variably enriched mantle wedge and contrasting melt types during arc stages following subduction initiation in Fiji and Tonga, southwest Pacific. *Earth and Planetary Science Letters* 335–336, 180–194. <https://doi.org/10.1016/j.epsl.2012.05.006>.
- Ulmer, P., 2001. Partial melting in the mantle wedge - the role of H₂O in the genesis of mantle-derived "arc-related" magmas. *Physics of the Earth and Planetary Interiors* 127, 215–232. [https://doi.org/10.1016/S0031-9201\(01\)00229-1](https://doi.org/10.1016/S0031-9201(01)00229-1).
- Vervoort, J.D., Blachert-Toft, J., 1999. Evolution of the depleted mantle: Hf isotope evidence from juvenile rocks through time. *Geochimica et Cosmochimica Acta* 63, 533–556. [https://doi.org/10.1016/S0016-7037\(98\)00274-9](https://doi.org/10.1016/S0016-7037(98)00274-9).
- Vervoort, J.D., Patchett, P.J., Blachert-Toft, J., Albarde, F., 1999. Relationships between Lu-Hf and Sm-Nd isotopic systems in the global sedimentary system. *Earth and Planetary Science Letters* 168, 79–99. [https://doi.org/10.1016/S0012-821X\(99\)00047-3](https://doi.org/10.1016/S0012-821X(99)00047-3).
- Waight, T., Baker, J., Peate, D., 2002. Sr isotope ratio measurements by double-focusing MC-ICPMS: techniques, observations and pitfalls. *International Journal of Mass Spectrometry* 221, 229–244. [https://doi.org/10.1016/S1387-3806\(02\)01016-3](https://doi.org/10.1016/S1387-3806(02)01016-3).
- Wang, C., 2011. Precambrian tectonic of South Margin of Tarim Basin, NW China (Ph.D. Thesis). Northwest University, Xi'an (123pp.).
- Wang, Y.H., Xiao, P.X., Pan, C.L., Sun, N.Y., Zhang, S.W., Li, J.X., 2002. The first disintegration of Altyn Tagh rock group and the characteristics of Altyn Tagh complexes. *Northwestern Geology* 35, 21–29.
- Wang, C.M., Zhang, L., Tang, H.S., Chen, H.Y., Li, X.L., Zheng, Y., Li, D.F., Fang, J., Dong, L.H., Qu, X., 2017. Genesis of the Kaladawan Fe-Mo ore field in Altyn, Xinjiang, China: constraints from mineralogy and geochemistry. *Ore Geology Reviews* 81, 587–601. <https://doi.org/10.1016/j.oregeorev.2016.09.001>.
- Wang, C.M., Zhang, L., Chen, H., Tang, H.S., Chen, Y.J., Dong, L.H., Qu, X., Zheng, Y., Li, D.F., Fang, J., 2018. Geochronology, geochemistry and tectonic significance of the ore-associated granites at the Kaladawan Fe-Mo ore field (Altyn), NW China. *Ore Geology Reviews* 100, 457–470. <https://doi.org/10.1016/j.oregeorev.2017.05.014>.
- Wang, C.M., Zheng, Y., Yu, P., 2018. Ore genesis and fluid evolution of the Kaladawan South Zn-Pb-Cu ore field, eastern Altyn Mountains (NW China): evidence from fluid inclusions, H-O isotopes and geochronology. *Ore Geology Reviews* 102, 300–312. <https://doi.org/10.1016/j.oregeorev.2018.09.011>.
- Weis, D., Kieffer, B., Maerschall, C., Barling, J., de Jong, J., Williams, G.A., Hanano, D., Pretorius, W., Mattielli, N., Scoates, J.S., Goolaerts, A., Friedman, R.M., Mahoney, J.B., 2006. High-precision isotopic characterization of USGS reference materials by TIMS and MC-ICP-MS. *Geochemistry, Geophysics, Geosystems* 7. <https://doi.org/10.1029/2006GC001283> (n/a–n/a).
- Winchester, J.A., Floyd, P.A., 1977. Geochemical discrimination of different magma series and their differentiation products using immobile elements. *Chemical Geology* 20, 325–343. [https://doi.org/10.1016/0009-2541\(77\)90057-2](https://doi.org/10.1016/0009-2541(77)90057-2).
- Woodhead, J.D., Herdt, J.M., Davidson, J.P., Eggins, S.M., 2001. Hafnium isotope evidence for "conservative" element mobility during subduction zone processes. *Earth and Planetary Science Letters* 192, 331–346. [https://doi.org/10.1016/S0012-821X\(01\)00453-8](https://doi.org/10.1016/S0012-821X(01)00453-8).
- Wu, J., Lan, C., Li, J., Yu, L., 2002. Geochemical evidence of MORB and OIB combination in Hongliugou ophiolite melanges. *Acta Petrologica et Mineralogica* 21, 24–30.
- Wu, F.Y., Yang, Y.H., Xie, L.W., Yang, J.H., Xu, P., 2006. Hf isotopic compositions of the standard zircons and baddeleyites used in U-Pb geochronology. *Chemical Geology* 234, 105–126. <https://doi.org/10.1016/j.chemgeo.2006.05.003>.
- Wu, C.L., Yao, S.Z., Zeng, L., Sen, Yang, J.S., Wooden, J.L., Chen, S.Y., Mazdab, F.K., 2007. Bashikaogong-Shimierbulake granitic complex, north Altun, NW China: geochemistry and zircon SHRIMP ages. *Science China Earth Sciences* 49, 1233–1251.
- Wu, C., Yang, J., Robinson, P.T., Wooden, J.L., Mazdab, F.K., Gao, Y., Wu, S., Chen, Q., 2009. Geochemistry, age and tectonic significance of granitic rocks in north Altun, northwest China. *Lithos* 113, 423–436. <https://doi.org/10.1016/j.lithos.2009.07.001>.

- j.lithos.2009.05.009.
- Wu, C.L., Xu, X.Y., Gao, Q.M., Li, X.M., Lei, M., Gao, Y.H., Frost, R.B., Wooden, J.L., 2010. Early Palaeozoic granitoid magmatism and tectonic evolution in North Qilian, NW China. *Acta Petrologica Sinica* 26, 1027–1044.
- Wu, Y., Chen, Z., Le, Chen, B.L., Wang, Y., Meng, L.T., He, J., Han, M.M., Wang, B., 2016. Geochronological and geochemical characteristics of the deformed diorite from the North Altyn brittle-ductile shear zone and its constraint on the Early Paleozoic tectonic evolution of the North Altyn Tagh. *Acta Petrologica Sinica* 32, 555–570.
- Xia, L.Q., Xia, Z.C., Yu, X.Y., 1996. Petrogenesis of Marine Volcanic Rocks in North Qilian, NW China. Geologic Publishing House, Beijing.
- Xia, L.Q., Xia, Z.C., Xu, X.Y., 2003. Magmagenesis in the Ordovician backarc basins of the Northern Qilian Mountains, China. *Geological Society of America Bulletin* 115, 1510–1522.
- Xiang, D., 1982. The characteristics of geological structures in the Chilienshan region, China. *Chinese J. Geol.* 25, 364–370.
- Xiao, W., Windley, B.F., Hao, J., Zhai, M., 2003. Accretion leading to collision and the Permian Solonker suture, Inner Mongolia, China: termination of the central Asian orogenic belt. *Tectonics* 22. <https://doi.org/10.1029/2002TC001484> (n/a–n/a).
- Xiao, W., Windley, B.F., Yong, Y., Yan, Z., Yuan, C., Liu, C., Li, J., 2009. Early Paleozoic to Devonian multiple-accretionary model for the Qilian Shan, NW China. *Journal of Asian Earth Sciences* 35, 323–333. <https://doi.org/10.1016/j.jseas.2008.10.001>.
- Xin, H.T., Liu, Y.S., Luo, Z.H., Song, S.C., Wang, S.Q., 2013. The growth of Archean continental crust in Aqitasgah Area of Southeast Tarim, China: Constraints from petrochemistry and chronology about Milan Group and TTG-gneiss. *Earth Science Frontiers* 20, 240–259.
- Xinjiang Bureau of Geology and Mineral Resources Exploration and Development, 2008. 1:250000 Geological Map of the Shimiankuang Area.
- Xinjiang Bureau of Geology and Mineral Resources Exploration and Development, 2009. Report for 1:50000 Regional Geologic Reconnaissance of the Kuoshubula Lake Area.
- Xinjiang Bureau of Geology and Mineral Resources Exploration and Development, 2009. Area, Report for 1:50000 Regional Geologic Reconnaissance of the Goukouquan Area.
- Xinjiang Bureau of Geology and Mineral Resources Exploration and Development, 2012. Report for Geological Reconnaissance in the Kaladawan Fe–Mo Deposit in Ruoqiang Country. Region, Xinjiang Uygur Autonomous.
- Xinjiang Bureau of Geology and Mineral Resources Exploration and Development, 2012. Report for Geological Reconnaissance in the Kaladaban Zn–Pb Deposit in Ruoqiang Country. Region, Xinjiang Uygur Autonomous.
- Xinjiang Bureau of Geology and Mineral Resources Exploration and Development, 2013. Report for Geological Reconnaissance in the Kaladaban West Cu–Zn–Pb Deposit in Ruoqiang Country. Region, Xinjiang Uygur Autonomous.
- Xiu, Q.Y., Yu, H.F., Liu, Y.S., Lu, S.N., Mao, D.B., Li, H.M., 2007. Geology and zircon U–Pb Age of pillow basalt at Qiashikansay in Northern Altyn Tagh, W China. *Acta Geologica Sinica* 81, 787–794.
- Xu, Z.Q., Xu, H.F., Zhang, J.X., Li, H., Bin, Zhu, Z.Z., Qu, J.C., Chen, D.Z., Chen, J.L., Yang, K.C., 1994. The Zhoulanglanshan Caledonian subductive complex in the northern Qilian Mountains and its dynamics. *Acta Geologica Sinica* 68, 1–15.
- Xu, Z., Yang, J., Zhang, J., Jiang, M., Li, H., Cui, J., 1999. A comparison between the tectonic units on the two sides of the Altyn sinistral strike-slip fault and the mechanism of lithospheric shearing. *Acta Geol. Sin. Ed.* 73, 193–205.
- Xu, Z., Yang, J., Wu, C., Li, H., Zhang, J., Qi, X., Song, S., Qiu, H., 2006. Timing and mechanism of formation and exhumation of the Northern Qaidam ultrahigh-pressure metamorphic belt. *Journal of Asian Earth Sciences* 28, 160–173. <https://doi.org/10.1016/j.jseas.2005.09.016>.
- Yang, Z.J., 2012. Early Palaeozoic Tectonic Evolution in Hongliugou, Altyn. Xinjiang, Chinese Academy of Geological Sciences.
- Yang, J.S., Xu, Z.Q., 2002. Subduction of continental crust in the Early Palaeozoic North Qaidam Ultrahigh-Pressure Metamorphic Belt, NW China: evidence from the discovery of coesite in the belt. *Acta Geol. Sin. Ed.* 76, 63–68.
- Yang, J., Wu, C., Shi, R., 2002. Sheeted dike swarm in Hongliugou, northwest of the region: evidence for seafloor spreading. *Geological Bulletin of China* 21, 69–74.
- Yang, J., Xu, Z., Zhang, J., Song, S., Wu, C., Shi, R., Li, H., Brunel, M., 2002. Early Palaeozoic North Qaidam UHP metamorphic belt on the north-eastern Tibetan Plateau and a paired subduction model. *Terra Nova* 14, 397–404. <https://doi.org/10.1046/j.1365-3121.2002.00438.x>.
- Yang, Y., Chen, X.H., Gehrels, G., Wang, X.F., Hong, Q., Chen, Z., Le, Feng, Y., Chen, B.L., Li, X.Z., 2004. Early Paleozoic magmatism and gold Metallogenesis in Altyn Mountains, Northwest China. *Mineralogical Deposita* 23, 464–472.
- Yang, J.S., Shi, R.D., Wu, C.L., Su, D.C., Chen, S.Y., Wang, X. Bin, Wooden, J., 2008. Petrology and SHRIMP age of the Hongliugou ophiolite at Milan, North Altun, at the Northern margin of the Tibetan plateau. *Acta Petrologica Sinica* 24, 1567–1584.
- Yang, Y., Wu, F., Xie, L., Zhang, Y., 2009. High-precision measurements of the 143Nd/144Nd isotope ratio in certified reference materials without Nd and Sm separation by multiple collector inductively coupled plasma mass spectrometry. *Analytical Letters* 43, 142–150. <https://doi.org/10.1080/00032710903276539>.
- Yin, A., Rumblehart, P.E., Butler, R., Cowgill, E., Harrison, T.M., Foster, D.A., Ingersoll, R.V., Zhang, Q., Zhou, X.Q., Wang, X.F., Hanson, A., Raza, A., 2002. Tectonic history of the Altyn Tagh fault system in northern Tibet inferred from Cenozoic sedimentation. *Bulletin Geological Society of America* 114, 1257–1295. [https://doi.org/10.1130/0016-7606\(2002\)114<1257:THOTAT>2.0.CO;2](https://doi.org/10.1130/0016-7606(2002)114<1257:THOTAT>2.0.CO;2).
- Yin, A., Manning, C.E., Lovera, O., Menold, C.A., Chen, X., Gehrels, G.E., 2007. Early Paleozoic Tectonic and Thermomechanical Evolution of Ultrahigh-Pressure (UHP) metamorphic rocks in the Northern Tibetan Plateau, Northwest China. *International Geology Review* 49, 681–716. <https://doi.org/10.2747/0020-6814.49.8.681>.
- Zartman, R.E., Doe, B.R., 1981. Plumbotectonics—the model. *Tectonophysics* 75, 135–162. [https://doi.org/10.1016/0040-1951\(81\)90213-4](https://doi.org/10.1016/0040-1951(81)90213-4).
- Zhang, J., Zhang, Z., Xu, Z., Yang, J., Cui, J., 2001. Petrology and geochronology of eclogites from the western segment of the Altyn Tagh, northwestern China. *Lithos* 56, 187–206. [https://doi.org/10.1016/S0024-4937\(00\)00052-9](https://doi.org/10.1016/S0024-4937(00)00052-9).
- Zhang, Z.C., Zhou, M.F., Robinson, P.T., Mao, J.W., Yang, J.M., Zuo, G.C., 2001. SHRIMP dating of the aoyougou ophiolite in the West sector of the North Qilian Mountains and its geological significance. *Acta Petrologica Sinica* 17, 222–226.
- Zhang, J., Meng, F., Yang, J., 2005. A New HP/LT metamorphic terrane in the Northern Altyn Tagh, Western China. *International Geology Review* 47, 371–386. <https://doi.org/10.2747/0020-6810-6814.47.4.371>.
- Zhang, J.X., Meng, F.C., Yu, S.Y., Chen, W., Chen, S.Y., 2007. $^{40}\text{Ar}/^{39}\text{Ar}$ geochronology of high-pressure/low-temperature blueschist and eclogite in the North Altyn Tagh and their tectonic implications. *Geology in China* 34, 558–564.
- Zhang, Z.W., Huang, G., Li, H.M., Zhang, W.F., 2012. LA-ICP-MS zircon U–Pb geochronology and geochemistry of gabbro and diorite from Qilesay pluton in Lapeiquan area of northern Altun Mountains and their tectonic implications. *Acta Petrologica et Mineralogica* 31, 13–27.
- Zhang, L., Unsworth, M., Jin, S., Wei, W., Ye, G., Jones, A.G., Jing, J., Dong, H., Xie, C., Le Pape, F., Vozar, J., 2015. Structure of the Central Altyn Tagh Fault revealed by magnetotelluric data: New insights into the structure of the northern margin of the India–Asia collision. *Earth and Planetary Science Letters* 415, 67–79. <https://doi.org/10.1016/j.epsl.2015.01.025>.
- Zhang, J., Yu, S., Li, Y., Yu, X., Lin, Y., Mao, X., 2015. Subduction, accretion and closure of Proto-Tethyan Ocean: early Paleozoic accretion/collision orogeny in the Altun–Qilian–North Qaidam orogenic system. *Acta Petrologica Sinica* 31, 3531–3554.
- Zhao, S., Li, S., Liu, X., Santosh, M., Somerville, I.D., Cao, H., Yu, S., Zhang, Z., Guo, L., 2015. The northern boundary of the Proto-Tethys Ocean: Constraints from structural analysis and U–Pb zircon geochronology of the North Qinling Terrane. *Journal of Asian Earth Sciences* 113, 560–574. <https://doi.org/10.1016/j.jseas.2015.09.005>.
- Zheng, Y.F., Wu, Y.B., Zhao, Z.F., Zhang, S.B., Xu, P., Wu, F.Y., 2005. Metamorphic effect on zircon Lu–Hf and U–Pb isotope systems in ultrahigh-pressure eclogite-facies metagranite and metabasite. *Earth and Planetary Science Letters* 240, 378–400. <https://doi.org/10.1016/j.epsl.2005.09.025>.
- Zheng, Y., Chen, Y., Dai, L., Zhao, Z., 2015. Developing plate tectonics theory from oceanic subduction zones to collisional orogens. *Science in China Series D: Earth Sciences* 58, 1045–1069. <https://doi.org/10.1007/s11430-015-5097-3>.
- Zhong, D.L., 1998. Paleo-Tethyan Orogenic Belt in West Sichuan and West Yunnan. Science Press, Beijing.
- Zhu, B.Q., Zhang, J.L., Tu, X.L., Chang, X.Y., Fan, C.Y., Liu, Y., Liu, J.Y., 2001. Pb, Sr, and Nd isotopic features in organic matter from China and their implications for petroleum generation and migration. *Geochimica et Cosmochimica Acta* 65, 2555–2570. [https://doi.org/10.1016/S0016-7037\(01\)00608-1](https://doi.org/10.1016/S0016-7037(01)00608-1).
- Zindler, A., Hart, S., 1986. Chemical Geodynamics. *Annual Review of Earth and Planetary Sciences* 14, 493–571.
- Zuo, G.C., Liu, J.C., 1987. The evolution of tectonics of early Paleozoic in North Qilian Range. *Scientia Geologica Sinica* 14–24.
- Zuo, G.C., Wu, H.Q., 1997. A Bisubduction-collision orogenic model of early-Paleozoic in the middle part of north Qilian area. *Advances in Earth Science* 12, 315–323.
- Zuza, A.V., Wu, C., Reith, R.C., Yin, A., Li, J., Zhang, J., Zhang, Y., Wu, L., Liu, W., 2017. Tectonic evolution of the Qilian Shan: an early Paleozoic orogen reactivated in the Cenozoic. *GSA Bulletin* 1–45. <https://doi.org/10.1130/B31721.1>.